The Same but Not the Same: The Case of (S)-Naproxen/cis-1-Amino-2-indanol Chiral Resolution via Diastereomeric Salt Formation

The same but not the same: the case of (S)-Naproxen / cis-1-Amino-2-indanol chiral resolution via diastereomeric salt formation

Journal:	*Crystal Growth & Design*
Manuscript ID	cg-2023-01313v.R2
Manuscript Type:	Article
Date Submitted by the Author:	n/a
Complete List of Authors:	Lippi, Martina; Universita degli Studi di Firenze, Industrial Engineering Rossi, Patrizia; Universita degli Studi di Firenze, Industrial Engineering Ceccarelli, Jacopo; Università degli Studi di Firenze, Experimental and Clinical Medicine Milazzo, Stella; Takeda Baxter Manufactoring Missina, Juliana; Hospital Israelita Albert Einstein Ienco, Andrea; ICCOM-CNR, Conti, Luca; Universita degli Studi di Firenze, Chemistry Ugo Schiff Chelazzi, Laura; Universita degli Studi di Firenze, Centro di Cristallografia Strutturale Paoli, Paola; Universita degli Studi di Firenze, Industrial Engineering

The same but not the same: the case of (S)-Naproxen / cis-1-Amino-2-indanol chiral resolution via diastereomeric salt formation

Martina Lippi,[a] Patrizia Rossi,[a,] Jacopo Ceccarelli,[a,b] Stella Milazzo,[a,c] Juliana Morais Missina,[a,d] Andrea Ienco,[e] Luca Conti,[f] Laura Chelazzi,[g] Paola Paoli[a]*

[a] = Department of Industrial Engineering, University of Florence, via Santa Marta 3, 50139 Florence (Italy); [b] = present address: Department of Experimental and Clinical Medicine, largo Brambilla 3, 50134 Florence, Italy; [c] = Present address: Takeda Baxter Manufactoring, via Giovan Battista Oliva 2, 56121 Pisa (Italy); [d] = Hospital Israelita Albert Einstein, 05529-060 São Paulo (Brazil); [e] = Consiglio Nazionale delle Ricerche, Istituto di Chimica dei Composti OrganoMetallici (CNR-ICCOM), via Madonna del Piano 10, 50019 Sesto F.no, Florence (Italy); [f] = Department of Chemistry "U. Schiff", University of Florence, via della Lastruccia 3, 50019 Sesto F.no, Florence (Italy); [g] = Centro di Cristallografia Strutturale, University of Florence, via della Lastruccia 3, 50019 Sesto F.no, Florence (Italy).

KEYWORDS

Active Pharmaceutical Ingredient, S-Naproxen, Aminoindanol, chiral resolution, diastereomeric salts, solid state investigation

ABSTRACT

The solid-state of four novel S-(+)-Naproxen (**S-Nap**) diastereomeric salts with cis-1-Amino-2-indanol (**SR-AI** and **RS-AI** enantiomers) are reported. The anhydrous **SR-AI_S-Nap_A** is the only obtained phase in the all the experimental conditions used, while the kinetically preferred diastereomeric salt **RS-AI_S-Nap_A1** forms only in certain conditions and underwent an irreversible phase transition to **RS-AI_S-Nap_A2** after melting; this second phase was obtained even by dehydration of the monohydrate salt **RS-AI_S-Nap_W**. The preferred crystallization of **SR-AI_S-Nap_A** was observed when **S-Nap** was introduced in a solution containing equimolar quantity of the racemic cis-1-Amino-2-indanol, in spite of the strict similarity of the crystal packings of **SR-AI_S-Nap_A** and **RS-AI_S-Nap_A1**.

With the aim of trying to explain the preference of **S-Nap** for the **SR-AI** enantiomer, an in-depth analysis and comparison of the diastereomeric salts crystal structures was carried out.

INTRODUCTION

More than half of Active Pharmaceutical Ingredients (APIs) are chiral, with at least one chiral centre,[1] and approximately 90% are marketed as racemic mixtures. Enantiomers in chiral environments exhibit distinct behaviors and interactions due to chiral discrimination. Consequently, in living systems, drug enantiomers commonly demonstrate stereoselectivity in pharmacokinetic processes such as absorption, distribution, metabolism, and elimination.[2] Typically, the desired therapeutic activity is confined to one enantiomer (eutomer), while the other (distomer) may be less potent and, on occasion, can yield a different pharmacological effect or be responsible for adverse effects.[1]

A well-known tragic case of enantiomeric toxicity concerned the drug thalidomide.[3] This event prompted the American Food and Drug Administration (FDA) to enhance regulation and monitoring of drugs containing chiral centers. Currently, as for chiral drugs, FDA and the European Medicines Agency (EMA) require strict controls of the synthetic procedure and impurities as well as rigorous investigations of the pharmacological and pharmacokinetic properties of each enantiomer along with its combination.[4,5]

Chirality has in pharmaceutical companies a huge relevance[13,14] that has led pharmaceutical companies to develop, whenever possible, new drugs as single enantiomers,[6–9] driven also by

advances in asymmetric synthesis and large-scale racemic separation tools. Quite recently several APIs, previously marketed as racemic mixtures, have been replaced by the corresponding eutomer, a process named “chiral switching” with the potential advantages of enhancing potency, selectivity and safety of the therapy as well as lowering patient drug dosage exposure; [10–12] Numerous methods for racemic separation based on chiral resolution are available (e.g., kinetic resolution, chromatographic resolution, membrane separation, crystallization), each with its own set of pros and cons.[15]

An economic, common and easy to scale-up method harnesses differences in solid state and solubility properties of diastereomeric salt pairs which lead to preferential precipitation of the least soluble one. Diastereomeric salts are formed by the reaction of the racemic mixture with an enantiomerically pure resolving agent in adequate conditions (solvent, temperature crystallization time, etc.). The resolving agents are enantiomerically pure molecules, preferentially of easy preparation, commercially available and cheap. This technique is particularly suitable for racemic compounds featuring ionizable groups such as amines and carboxylic acids.[16–21]

Choosing the most appropriate resolving agent can be tricky and time-consuming, so that it is often widely empirical. X-ray diffraction, along with various thermoanalytical techniques and

in-silico approaches, serves as essential tools for exploring the forces and interactions in crystal packing,[22-30] hence playing a crucial role in understanding the driving forces behind the formation of structurally related diastereomeric salts.[31-33]

As part of our ongoing structural investigations of Non-Steroidal Anti-Inflammatory Drugs (NSAIDs) solid forms,[34–37] we have recently reported on the diastereomeric salts of naproxen (Nap), ibuprofen (Ibu), and ketoprofen (Ket) (Scheme 1) with (*R*)-(+)- and (*S*)-(-)-1-phenylethylamine (PEA).[38] Nap, Ibu and Ket are 2-arylpropionic acid derivatives containing a stereocenter in the α-position, commonly used for the treatment of pain and inflammatory conditions (e.g rheumatoid arthritis, postoperative surgical conditions, menstrual cramps).[39–42] According to our study, S-Ket and S-Ibu preferentially capture the homochiral PEA (whereas S-Nap is not selective). All the salts share 2_1-columns, each column consisting of NSAID and 1-phenylthylammonium ions assembled *via* the 1-phenylethylammonium-carboxylate supramolecular heterosynthon. We speculated that the planar boundary surfaces,[43] which characterize the supramolecular sheets formed by the NSAID/PEA columns inside the crystals of the S-Ket and S-Ibu homochiral salts, favoring a close packing, are responsible of the higher stability of these DSs with respect to that of the corresponding heterochiral ones.

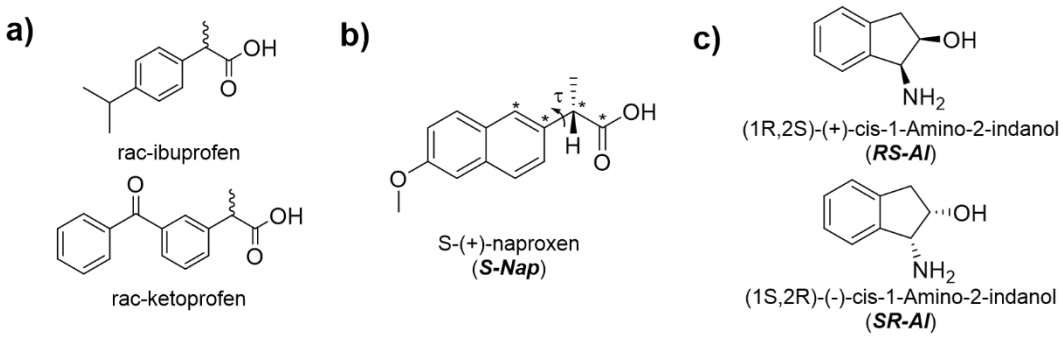

Scheme 1. a) Schematical drawing of ibuprofen and ketoprofen; b) Schematical drawing of (S)-(+)-Naproxen (**S-Nap**) with evidenced the atoms defining the torsion angle τ; c) Schematical drawing of (1R,2S)-(+)-*cis*-1-Amino-2-indanol (**RS-AI**) and (1S,2R)-(-)-*cis*-1-Amino-2-indanol (**SR-AI**).

The fact that **S-Nap** is not selective (2_1 sheets of both salts are characterized by almost planar boundary surfaces) prompted us to further investigate its behavior towards diastereomeric salt formation. As chiral agent was chosen the *cis*-1-Amino-2-indanol molecule,[44] whose pure enantiomers are good resolving agents for Ibu and Ket.[17] For example S-Ket selectively crystallized by using (1R,2S)-1-Amino-2-indanol (Scheme 1c, **RS-AI**, hereafter); while the use of (1S,2R)-1-Amino-2-indanol (Scheme 1c, **SR-AI**, hereafter) led to the selective crystallization of R-Ket. Moreover, solubility studies showed that DSs of S-Ket and R-Ket with aminoindanols display larger solubility differences with respect to those with other chiral

amines. The structural aspects of racemic 2-arylalkanoic acids resolution by using 1-Amino-2-indanol as resolving agents have been investigated by Kinbara and coworkers.[45,46] In their article they reported, for example, that the rigid relative configuration of the enantiopure **SR-AI** enhances the resolution efficiency for racemic 2-arylalkanoic acids, by promoting the formation of a supramolecular hydrogen-bonded column.[45] According to Kinbara, the chiral discrimination primarily relies on hydrogen bonding interactions, with CH···π interactions also playing a contributing role. The differential stability between less and more soluble diastereomers is attributed to variations in the strength of these interactions. The relative arrangement of the ammonium, hydroxy, and aromatic groups in the resolving agent seems to significantly influence the crystal stabilization, as they found that the ammonium and aromatic groups are pivotal in forming the columnar network while the role of the hydroxy group varies based on its orientation. Another paper[46] by the same author, dealing with *trans*-1-Amino-2-indanol and *trans*-2-Amino-1-indanol towards 2-arylalkanoic acids, confirmed that the ability of aminoindanols to resolve racemic acids is markedly influenced by the relative configuration and positioning of hydrogen-bonding groups. These factors impact the stability of the less soluble salt, influencing preferential crystallization.

As a whole *trans*-1-Amino-2-indanol showed a high chiral resolution ability towards 2-arylalkanoic acids having a naphthyl group in α-position, including naproxen ((S)-(+)-Naproxen is the major enantiomer).

To explore the preference of (S)-(+)-Naproxen (**S-Nap**, Scheme 1) for one of the cis-1-Amino-2-indanol enantiomers (see Scheme 1) and gain insights into the forces driving the chiral discrimination process, we present here a comprehensive experimental and in-silico analyses of diastereomeric salts. Specifically, we focus on the solid forms of (S)-(+)-Naproxen with (1S,2R)-(-)-*cis*-1-Amino-2-indanol (**SR-AI**) and (1R,2S)-*cis*-(+)-1-Amino-2-indanol (**RS-AI**). The results illuminate potentially significant, even subtle, differences in the S-Nap/AI diastereomeric salts from a solid-state perspective. Additionally, we discuss the monohydrated form of the diastereomeric salt with **RS-AI** and explore the relationships between the various solid forms of this salt.

EXPERIMENTAL SECTION

Chemicals

(2*S*)-2-(6-methoxynaphthalen-2-yl)propanoic acid ((S)-(+)-Naproxen, 99%) was purchased from Alfa Aesar. (1S,2R)-(-)-cis-1-Amino-2-indanol (99%) and (1R,2S)-(+)-cis-1-Amino-2-

indanol (99%) were purchased from abcr GmbH. All the compounds were used without any further purification.

Procedure for salt preparation

All single crystal samples (SCs) were obtained using ultrapure water (Milli-Q, Millipore type 1, 18.2 MΩcm resistivity at 25˚C) and/or ethanol (96%) purchased from Sigma-Aldrich.

For the liquid assisted grinding (LAG) experiments a Retsch MM200 mixer mill, operating at a frequency of 20 Hz for 20 minutes, was used. In all the LAG experiments zirconium oxide grinding jars and three zirconium oxide balls were used.

In all the tests reported below, 1 mmol of (S)-(+)-Naproxen (230.3 mg) and 1 mmol of cis-1-Amino-2-indanol [(1S,2R) or (1R,2S), 142.1 mg] were used.

Finally, the PXRD pattern of each microcrystalline sample (MP) was compared to the theoretical one of the corresponding single-crystal (SC) phase (**SR-AI_S-Nap_A**, **RS-AI_S-Nap_A1**, **RS-AI_S-Nap_A2** and **RS-AI_S-Nap_W**) to confirm the content in terms of crystalline phase of the obtained powder (superimposition of the theoretical and experimental PXRD patterns are reported in SI Figures S1- S4).

Synthesis of (1S,2R)-(-)-cis-1-Ammonio-2-indanol (2S)-2-(6-methoxynaphtalen-2-yl)propionate (**SR-AI_S-Nap_A**)

SC: three procedures were followed to obtain **SR-AI_S-Nap_A** SCs:

1) (S)-(+)-Naproxen and (1S,2R)-(-)-cis-1-Amino-2-indanol were dissolved in EtOH (8 mL) at rt, and then H_2O (2 mL) was added. After few minutes colorless needle-like crystals started to form;

2) (S)-(+)-Naproxen and (1S,2R)-(-)-cis-1-Amino-2-indanol were dissolved in 10 mL of a 80% mixture of EtOH/H_2O, then the solution was left under stirring for 1h at reflux. After cooling colorless needle-like crystals formed;

3) (S)-(+)-Naproxen and (1S,2R)-(-)-cis-1-Amino-2-indanol were suspended in 9 mL of a 2:1 EtOH/H_2O solution and heated at 70 ˚C under stirring until the total dissolution of the solid. On cooling the solution, the slowly formation of colorless needles was observed.

MPs: 2 different procedures were used to obtain microcrystalline powder samples of this salt:

1) (S)-(+)-Naproxen and (1S,2R)-(-)-cis-1-Amino-2-indanol were introduced in the mixer mill and 2-3 drops of EtOH were added. At the end of a 20-minute grinding, the formation of the **SR-AI_S-Nap_A** salt was observed;

2) (S)-(+)-Naproxen and (1S,2R)-(-)-cis-1-Amino-2-indanol were introduced in the mixer mill and 2-3 drops of water were added. At the end of a 20-minute grinding, the formation of the **SR-AI_S-Nap_A** salt was observed.

Synthesis of (1R,2S)-(+)-cis-1-Ammonio-2-indanol (2S)-2-(6-methoxynaphtalen-2-yl)propionate (**RS-AI_S-Nap_A1**)

SC: two procedures were followed to obtain **RS-AI_S-Nap_A1** SCs:

1) S-(+)-Naproxen and (1R,2S)-(+)-cis-1-Amino-2-indanol were dissolved in EtOH (8 mL) at rt, and then H_2O (2 mL) was added. After few minutes colorless needle-like crystals started to form.

2) S-(+)-Naproxen and (1R,2S)-(+)-cis-1-Amino-2-indanol were dissolved in 10 mL of a 80% mixture of EtOH/H_2O, then the solution was left under stirring for 1h at reflux. After cooling colorless needle-like crystals formed.

MP: S-(+)-Naproxen and (1R,2S)-(+)-cis-1-Amino-2-indanol were introduced in the mixer mill and 2-3 drops of EtOH were added. At the end of a 20-minute grinding, the formation of **RS-AI_S-Nap_A1** salt was observed.

Synthesis of (1R,2S)-(+)cis-1-Ammonio-2-indanol (2S)-2-(6-methoxynaphtalen-2-yl)propionate hydrate (**RS-AI_S-Nap_W**)

SC: S-(+)-Naproxen and (1R,2S)-(+)-*cis*-1-Amino-2-indanol were suspended in 9 mL of a 2:1 EtOH/H_2O solution and heated at 70 ˚C under stirring until the total dissolution of the solid. Cooling the solution, the slowly formation of colorless needles was observed.

MP: S-(+)-Naproxen and (1R,2S)-(+)-*cis*-1-Amino-2-indanol were introduced in the mixer mill and 2-3 drops of H_2O were added. After 20 minutes of grinding, the **RS-AI_S-Nap_W** salt was formed.

Single-Crystal X-ray Diffraction (SCXRD)

SCXRD data of **SR-AI_S-Nap_A**, **RS-AI_S-Nap_A1** and **RS-AI_S-Nap_W** were collected on a Bruker Apex-II diffractometer equipped with a CCD detector (T = 100 K, Cu−Kα radiation (λ = 1.54178 Å). Data were collected with the Bruker APEX2 software[47], while data integration and reduction were performed with the Bruker SAINT software. [48] The crystal structures were solved using the SIR-2004 package[49] and refined by full-matrix least squares against F2 using all data (SHELXL-2018/3).[50] All the non-hydrogen atoms of the three structures, were refined with anisotropic displacement parameters; concerning the hydrogen atoms, those of the

anhydrous compounds (**SR-AI_S-Nap_A** and **RS-AI_S-Nap_A1**) were found in the Fourier difference maps and their coordinates were freely refined while their thermal parameters were set in accordance with that of the atoms to which they are bonded. In the hydrated compound **RS-AI_S-Nap_W**, the hydrogen atoms bonded to carbon atoms were put in calculated position, while all the other ones were found in the Fourier difference maps, their coordinates were freely refined while their thermal parameter was set in accordance with that of the atoms to which they are bonded. During the refinement of **SR-AI_S-Nap_A** and **RS-AI_S-Nap_W**, dfix and dang instructions (parameters set in accordance to the X-H value at 100K) were used for the 1-Amino-2-indanol N-H distances and angles, in both salts, and also for the water O-H distances and angles in **RS-AI_S-Nap_W**. Geometrical calculations were performed by PARST97[51] and molecular plots were produced by the program CCDC Mercury (v. 2022.3.0).[52]

Figure 1 shows the ORTEP views together with the atom labelling of the **SR-AI_S-Nap_A**, **RS-AI_S-Nap_A1** and **RS-AI_S-Nap_W** asymmetric unit, as well as that of **RS-AI_S-Nap_A2** whose structure was solved by using PXRD data (see below). In Table 1 crystallographic data and refinement parameters of the four structures are reported.

Table 1. Crystallographic Data and Refinement parameters for **SR-AI_S-Nap_A**, **RS-AI_S-Nap_A1**, **RS-AI_S-Nap_A2** and **RS-AI_S-Nap_W**

	SR-AI_S-Nap_A	**RS-AI_S-Nap_A1**	**RS-AI_S-Nap_A2**	**RS-AI_S-Nap_W**
Moiety formula	$(C_9H_{12}NO)(C_{14}H_{13}O_3)$	$(C_9H_{12}NO)(C_{14}H_{13}O_3)$	$(C_9H_{12}NO)(C_{14}H_{13}O_3)$	$(C_9H_{12}NO)(C_{14}H_{13}O_3)(H_2O)$
Formula weight	379.44	379.44	379.44	397.45
T (K)	100	100	300	100
Crystal system, space group	Monoclinic, $P2_1$	Monoclinic, $P2_1$	Orthorhombic, $P2_12_12_1$	Monoclinic, $P2_1$
Unit cell dimensions (Å, °)	a = 11.0775(9) b = 6.3903(5), β = 94.704(6)	a = 11.0114(6) b = 6.4629(3), β = 100.809(2)	a = 37.152(1) b = 5.9829(1)	a = 16.6585(12) b = 6.2504(4), β = 109.374(4)

	c = 13.761(1)	c = 14.0469(7)	c = 9.1733(2)	c = 21.1989(14)
V(Å^3)	970.9(1)	981.92(9)	2039.01(1)	2082.3(2)
Z, d_{calc}(g/cm^3)	2, 1.298	2, 1.283	4, 1.236	4, 1.268
μ (mm^{-1})	0.715	0.707	---	0.726
F(000)	404	404	---	848
Reflections collected/unique/R_{int}	11704 / 3722 / 0.0943	20362 / 3821 / 0.0858	---	23165 / 7487 / 0.1003
Data/parameters	3722 / 328	3821 /328	---	7487 /560
Final R indices [I>2σ(I)]	R1 = 0.0612, wR2 = 0.1584	R1 = 0.0481, wR2 = 0.1274	---	R1 = 0.0806, wR2 = 0.2056

R indices all data	R1 = 0.0800, wR2 = 0.1799	R1 = 0.0506, wR2 = 0.1297	---	R1 = 0.1087, wR2 = 0.2436
Rwp (%)	---	---	0.0675	---
GOOFs	1.059	1.162	1.89	1.006

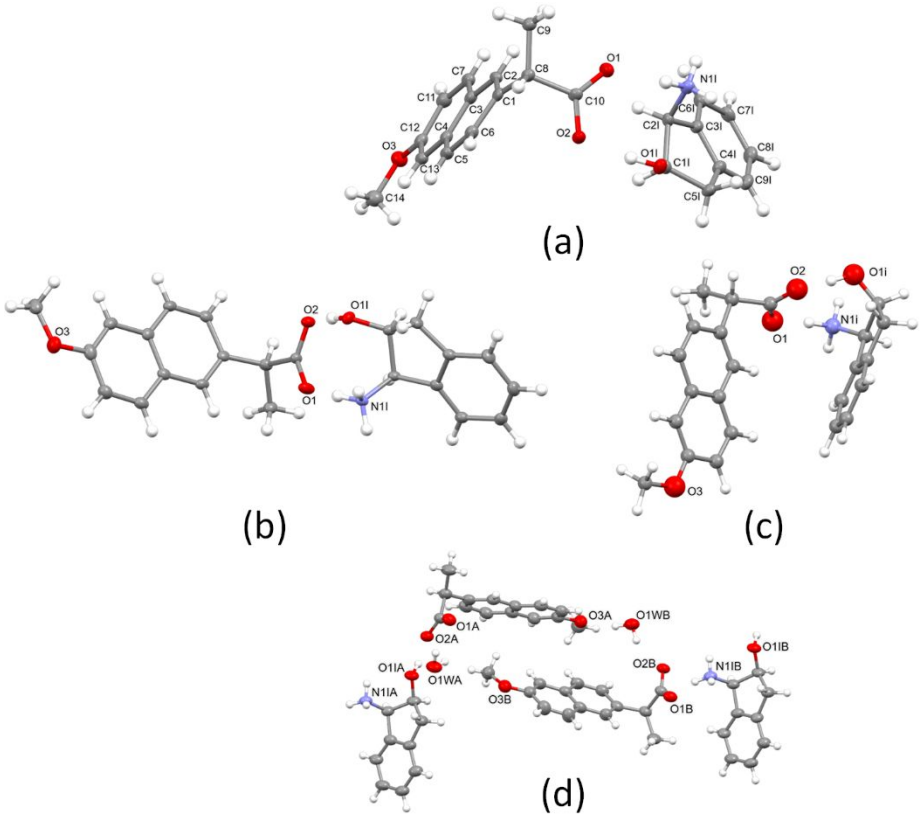

Figure 1. Views of the asymmetric unit of **SR-AI_S-Nap_A** (a), **RS-AI_S-Nap_A1** (b), **RS-AI_S-Nap_A2** (c) and **RS-AI_S-Nap_W** (d). For **SR-AI_S-Nap_A**, **RS-AI_S-Nap_A1** and **RS-AI_S-Nap_W** ORTEP views with 50% ellipsoid probability are shown, while for **RS-AI_S-Nap_A2** a

ball and stick model is used. The atoms labelling scheme adopted is the same for all the structures and, for the sake of clarity, reported (except for the hydrogen atoms) only for **SR-AI_S-Nap_A**, while in the other three structures just the nitrogen and oxygen labels are shown.

Powder X-ray Diffraction (PXRD)

All the room temperature PXRD measures were carried out by using a Bruker New D8 Da Vinci diffractometer (Cu-Kα radiation = 1.54056Å, 40 kV x 40 mA), equipped with a Bruker LYNXEYE-XE detector, scanning range 2θ = 3-40˚, 0.03˚ increments of 2θ and counting time of 0.8 s/step.

The structure determination of **RS-AI_S-Nap_A2** was performed by using high-quality PXRD data recorded in a 0.3 mm glass capillary at room temperature (scanning range 2θ = 3–70˚, 0.01˚ increments of 2θ, and a counting time of 1536 s total time/step).The space group was determined with EXPO2014[53] ($P2_12_12_1$ with Z=4), then simulated annealing (EXPO2014 suite) was used to solve the structure. Each annealing trial works on three runs with a cooling rate (Tn/Tn−1) of 0.95. All the torsion angles were allowed to rotate freely during the refinement process while bond distances and angles were kept fixed. The best solution was chosen as starting geometry for a fixed cell optimization using HSE-3c functional[54] using Crystal17.[55] The optimized model was used for Rietveld refinement, which was performed with the software TOPASv6.[56] Background and peak shape were fitted using a shifted Chebyshev function with eight coefficients and a Pseudo-Voigt function, respectively. All atoms were isotropically refined with a typical thermal parameter depending on the element. All the

hydrogen atoms were fixed in calculated positions. Crystal data and refinement parameters are reported in Table 1.

In-silico analysis

The crystal packing of **SR-AI_S-Nap_A**, **RS-AI_S-Nap_A1, RS-AI_S-Nap_A2** and **RS-AI_S-Nap_W** was analyzed with CCDC Mercury (v. 2022.3.0).[52] Crystal-Explorer17[57] was used to compute the Hirshfeld surfaces (HS) and their associated 2D fingerprint plots in order to further investigate the intermolecular interactions which hold together the crystal of the four diastereomeric salts.

Cambridge Structural Database Survey.

The web version of the Cambridge Structural Database[58] was searched for crystal structures containing the 1-Amino-2-indanol fragment (Scheme 2) to get information about preferred H-bond and packing motifs. Crystal structures containing the naproxen skeleton were also searched for.

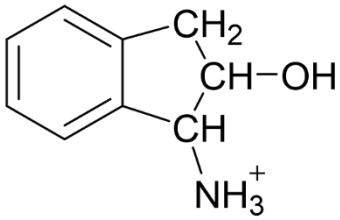

Scheme 2. 1-Amino-2-indanol fragment searched in the Cambridge Structural Database.

Differential scanning calorimetry (DSC)

Differential Scanning Calorimetry (DSC) experiments were performed by using a Mettler Toledo DSC1 Excellence instrument. Measurements were run in aluminum pans with pinhole lids (samples' mass ranged from 0.7 to 3.5 mg). Temperature and enthalpy calibrations were done by using indium as standard. Measurements were carried out in the 40-200˚C temperature range and a linear heating rate of 10˚C/min was used. Experiments were performed in air. DSC peaks were analyzed using the STARe software.[59] The reported data were the average of two measurements, and standard errors were ±0.1˚C for temperature and ±0.3 kJ/mol for enthalpy.

Solid Forms Stability Assessment

The stability towards the water uptake of the three anhydrous diastereomeric salts **SR-AI_S-Nap_A**, **RS-AI_S-Nap_A1** and **RS-AI_S-Nap_A2**, as well as the dehydration propensity of the hydrated salt **RS-AI_S-Nap_W** were tested as follow:

-Hydration tests-

1) the anhydrous salts (**SR-AI_S-Nap_A**, **RS-AI_S-Nap_A1** and **RS-AI_S-Nap_A2**) were kept in a desiccator at constant relative humidity (ca. 75% by using a saturated solution of NaCl) for a week;

2) a sample of each anhydrous salt (20 mg) was ground for five minute with a drop of water. The resulting powders were left standing at rt and ambient pressure for 1 hour;

3) 50 mg of each salt were put in a vial with 5 mL of water. The slurries were kept under stirring for 1 hour at r.t.

In all cases the PXRD patterns were collected and compared with those taken at the beginning of the experiment.

-Dehydration test-

The dehydration process of the **RS-AI_S-Nap_W** salt was investigated by keeping a microcrystalline sample of this salt in the oven for 20 minutes at 140˚C. PXRD patterns were collected at the beginning and at the end of the experiment and compared.

Selective crystallization tests.

Different procedures were employed for the selective crystallization tests (in all cases 1 mmol of **S-Nap**, 230.3 mg, and 1 mmol of each *cis*-1-Amino-2-indanol [**SR-AI** and **RS-AI**, 142.1 mg] were used):

1) **S-Nap** was added to an equimolar solution of **SR-AI** and **RS-AI** in 10 mL of a 80% mixture of EtOH/water. The solution was left under stirring for 1h at reflux. The reflux was then turned off and the solution was let to return to room temperature. As soon as the solution reached r.t. colorless needles formed. The sample was filtered and dried in open air overnight (sample weight = 322.5 mg, yield = 85%);

2) **S-Nap** was added to an equimolar solution of **SR-AI** and **RS-AI** in 8 mL of EtOH. Then, under stirring at r.t., 2 mL of water were added. Within the first five minutes colorless needles precipitated. The sample was filtered and dried in open air overnight (sample weight = 337.7 mg, yield = 89%);

3) **S-Nap** was added to an equimolar solution of **SR-AI** and **RS-AI** in 9 mL of a 2:1 EtOH/H_2O solution and heated at 70 ˚C under stirring until the total dissolution of the solid. The solution was let to cool to room temperature, and the slow formation of colorless needles was observed.

After a couple of days, the sample was filtered and dried in open air overnight (sample weight = 265.6 mg, yield = 70%);

In all the three cases, the PXRD pattern of the sample obtained by precipitation evidenced the formation of the **SR-AI_S-Nap-A** diastereomeric salt.

RESULTS

Procedure for salts preparation.

For the preparation of SCs samples of **SR-AI_S-Nap_A**, **RS-AI_S-Nap_A1** and **RS-AI_S-Nap_W,** three solution-based procedures were used. Concerning the formation of the SR-AI/S-Nap salt, changes in the experimental conditions (temperature: 25 or 70˚C; solvent composition: 4:1 or 2:1 EtOH:H_2O; stirring at r.t. or at 70˚C, for few minutes or 1 hour at reflux) did not influence the result and, in all cases, the **SR-AI_S-Nap_A** phase was obtained. On the contrary, in the case of the RS-AI/S-Nap salt, the change of solvent composition led to the formation of two different phases, *i.e.* the presence and the amount of the water during the crystallization process plays a critical role in the formation of the hydrated (**RS-AI_S-Nap_W**) or the anhydrous (**RS-AI_S-Nap_A1**) salt (see Experimental Section).

Changes in temperature (r.t. or 70˚C) or in the general conditions of the experiment (stirring at r.t., or at 70˚C, for few minutes of for 1 hour at reflux) did not influence the result.

The importance of the quantity of water, in driving the formation of the hydrate or anhydrous phases of the RS-AI/S-Nap salts, is confirmed by the synthesis of the MCs samples. In fact, while all the LAG experiments resulted in the **SR-AI_S-Nap_A** phase (see Figures S1-S2), **RS-AI_S-Nap_A1** was obtained when ethanol is used in the LAG procedure, while the use of water led to the formation of **RS-AI_S-Nap_W** (see Figures S3-S4).

Finally, **RS-AI_S-Nap_A2** was obtained only for dehydration of the hydrated phase **RS-AI_S-Nap_W** in oven at 140˚C (see Figure S5 and "Solid Forms Stability Assessment" paragraph).

Solid Forms Stability Assessment

The solid forms behavior of the S-Nap/AI salts was investigated by powder X-ray diffraction (PXRD) and DSC analyses (see scheme 3).

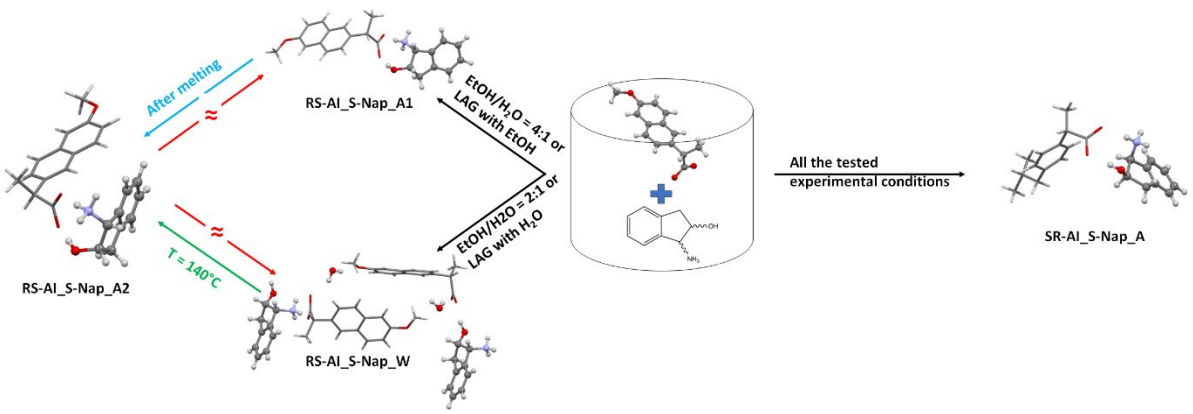

Scheme 3. Solid forms formation conditions and relationships.

The anhydrous **SR-AI_S-Nap_A** compound is stable from r.t to melting, as provided by the DSC curve (collected in the r.t.-200˚C range) which revealed just one endothermic event, related to the melting of the compound (peak = 183.8˚C, extrapolated peak = 183.7˚C, onset = 183.5˚C, ΔH = 85.7 kJ/mol, Figure S6). Considering that the PXRD pattern collected at r.t. well superimposes with the theoretical one obtained by the SCXRD data collected at 100K, we can assume that the stability range for this phase is from -170˚C to melting (184˚C).

Different was the behavior of the diastereomeric solid form **RS-AI_S-Nap_A1**. In fact, in the same temperature range, its DSC curve showed three thermal events (Figure S7): a first endothermic peak (peak = 164.0˚C, extrapolated peak = 164.1˚C, onset = 163.9˚C, ΔH = 37.9 kJ/mol) is immediately followed by an exothermic one (peak = 166.4˚C, extrapolated peak = 166.7˚C, onset = 166.4˚C) and then by a second endothermic peak (peak = 175.9˚C, extrapolated peak = 175.9˚C, onset = 175.8˚C). These three events were tentatively attributed to the melting of **RS-AI_S-Nap_A1** (first endothermic peak), the recrystallization of a second phase (exothermic peak), followed by its melting (second endothermic peak). On cooling no further thermal events were observed. The formation of a new anhydrous phase (**RS-AI_S-**

Nap_A2) has been confirmed by the comparison of the PXRD pattern of a sample of **RS-AI_S-Nap_A1** kept in oven at 165˚C for half an hour with the theoretical one as obtained from the SCXRD data **RS-AI_S-Nap_A1** (Figure 2). In Figure S8 the DSC curve of **RS-AI_S-Nap_A2** is reported (peak = 175.1˚C, extrapolated peak = 175.1˚C, onset = 173.7˚C, ΔH = 56.0 kJ/mol) Moreover, due to the good quality of the polycrystalline solid form obtained from this experiment, its crystal structure was solved (see Table 1, Powder X-Ray Diffraction and Molecular and Crystal Structures from SCXRD and PXRD chapters for details).

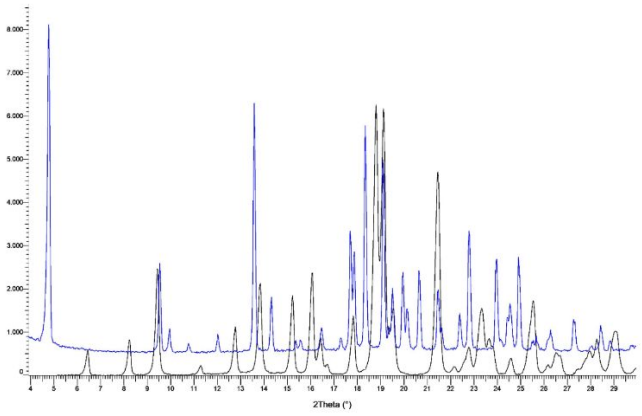

Figure 2. Superimposition of the PXRD pattern of RS-AI_S-Nap at the beginning (black) and at the end (blue) of the oven experiment.

As for the hydrated salt (**RS-AI_S-Nap_W**), its DSC curve showed two endothermic events: the first one (peak = 129.6˚C, extrapolated peak = 130.1˚C, onset = 129.6˚C, ΔH = 16.6 kJ/mol) which can be related to the loss of water; while the second, due to the melting of the resulting anhydrous compound, occurred at about 175˚C (peak = 175.9˚C, extrapolated peak = 175.9˚C, 175.9˚C, ΔH = 51.9 kJ/mol, Figure S9), *i.e.* the same melting temperature of **RS-AI_S-Nap-A2**. To confirm that dehydration the hydrated phase **RS-AI_S-Nap_W** gave **RS-AI_S-Nap_A2**, a sample of **RS-AI_S-Nap_W** was put in an oven at 140˚C (i.e. above its dehydration temperature as obtained by DSC analysis); the comparison of the PXRD patterns of **RS-AI_S-Nap-A2** and that collected from the resulting solid form at the end of the experiment evidenced that actually they have the same crystalline phase (see Figure S5).[60]

Finally, all the anhydrous phases are stable towards re-hydration in the adopted experimental conditions.

Molecular and Crystal Structures from Single-Crystal and Powder X-ray Diffraction

The **S-Nap** anion adopts an almost identical conformation in **SR-AI_S-Nap_A** and **RS-AI_S-Nap_A1**, with the carboxylate group almost perpendicular to the aryl moiety, while in **RS-**

AI_S-Nap_A2 it is eclipsed, being the values of the C6-C1-C8-C10 torsions angle τ (see Scheme 1 and Figure S10) -82.3(5), -80.3(4) and -24.9(4)˚, respectively.

The asymmetric unit of the anhydrous diastereomeric salts **SR-AI_S-Nap_A**, **RS-AI_S-Nap_A1** and **RS-AI_S-Nap_A2** contains one naproxen anion and one 1-Amino-2-indanol cation (**AI** in the following), which interact *via* NH···OOC and OH···OOC hydrogen bonds originating, according to graph set notation,[61] a $R_2^2(9)$ motif (Figure 3 left, Table 2). This ionic pair replicates along the *b*-axis held together by NH···OOC bonds (the NH_3^+ group acts as H-bond donor towards two contiguous naproxen anions related by translation (see Figure 3 left and Table 2) and 2_1-related aminoindanol cations which bridge contiguous **AI** cations (the hydroxyl group works in this case as H-bond acceptor) resulting in an $R_4^3(11)$ H-bond pattern (Figure 3 left). Obviously, these **AI** cations (Figure 2 left) in turn describe $R_2^2(9)$ motifs with 2_1-related naproxen anions. In **RS-AI_S-Nap_A2**, both the H-bond ring motifs ($R_2^2(9)$ and $R_4^3(11)$), based on the related D···A bond distances (Table 2), appear definitely more stable with respect to that found in the **RS-AI_S-Nap_A1** polymorph as well as in the diastereomeric salt **SR-AI_S-Nap_A**.

In summary the **AI** ammonium group acts as H-bond donor towards two **S-Nap** anions related by translation and the hydroxyl group of an **AI** cation symmetry related by the 2_1- screw axis

which in turn binds a 2_1 symmetry related **S-Nap** anion (Figure 3), originating a H-bonded column which extends along the b-axis direction.

All the potential hydrogen bond donors/acceptors play a role in constructing each column. The hydroxyl group works as donor and acceptor, while the carboxylate oxygen atoms act as bifurcated acceptor (towards two aminoindanol cations and, as for O1, towards CH donors provided by contiguous naproxen anions).

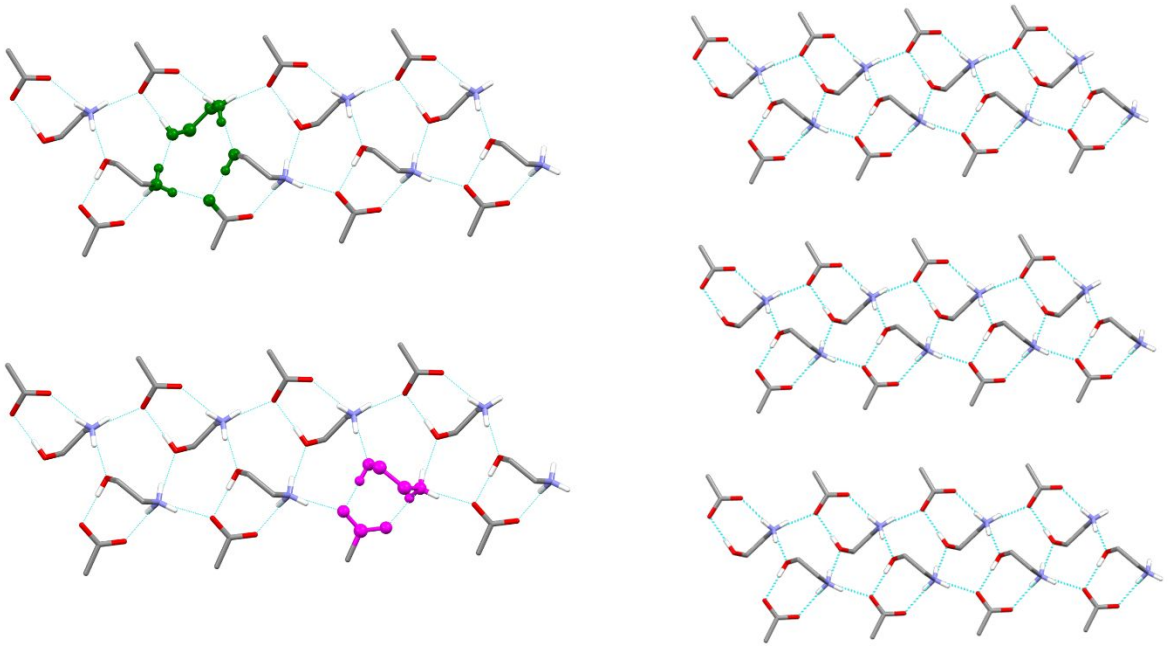

Figure 3. Schematic drawing of the H-bond network in the naproxen diastereomeric salts evidencing the $R_2^2(9)$ (ball and stick, pink) and $R_4^3(11)$ (ball and stick, green) H-bond motifs view along the *a*-axis direction. Left: columnar H-bond network; right: columns packing. Figure refers to **SR-AI_S-Nap_A**.

Finally, each naproxen anion acts as H-bond acceptor, via the carboxylate group, towards two aminoindanol cations and *vice versa* for the cation which additionally works as H-bond donor ($-NH_3^+$) and acceptor (-OH) towards two symmetry related cations.

Table 2. Selected H-bond distances and angles in **SR-AI_S-Nap_A** and **RS-AI_S-Nap_A1** and **RS-AI_S-Nap_A2**

X-H···Y	X···Y (Å)	H···Y (Å)	X-H···Y (°)
SR-AI_S-Nap_A			
N1-H1NA···O1	2.737(5)	1.90(4)	159(4)
O1I-H1O···O2	2.641(5)	1.75(7)	167(7)
N1-H1NB···O2[1]	2.737(5)	1.87(3)	166(3)
N1-H1NC···O1I[2]	2.825(6)	1.97(5)	167(4)
RS-AI_S-Nap_A1			
N1I-H1NA···O1	2.729(4)	1.87(4)	154(4)
O1I-H1OI···O2	2.657(3)	1.72(4)	172(4)
N1I-H1NB···O2[3]	2.786(4)	1.84(5)	165(4)
N1I-H1NC···O1I[4]	2.819(4)	1.84(5)	167(4)
RS-AI_S-Nap_A2			

N1I-H1NA···O1	2.537(3)	1.439(3)	168(4)
O1I-H1OI···O1[1]	2.540(3)	1.531(4)	179(4)
N1I-H1NB···O2[1]	2.667(3)	1.595(4)	176(3)
N1I-H1nc···O1I[5]	2.745(4)	1.727(3)	161(4)

[1]=x, 1+y, z; [2]=-x,0.5+y,1-z; [3]=x, -1+y, z; [4]=1-x, -0.5+y,1-z; [5]=-x, -0.5+y, -0.5-z

As well highlighted in Figure 4 (right), with respect to the H-bonded $R_2^2(9)$ ring, the aromatic moieties of the charged partners are *anti* disposed in **RS-AI_S-Nap_A1** and *syn* oriented in **SR-AI_S-Nap_A** and **RS-AI_S-Nap_A2**. Irrespective of the *anti* and *syn* orientation, in **RS-AI_S-Nap_A1** and **SR-AI_S-Nap_A** each H-bonded column is further reinforced by CH···π interactions between facing **AI** and naproxen ions (C6I-H6I···centroid distance 3.06(6)Å, angle 164(3)˚ and C5I-H5I2···centroid distance 3.06(5)Å, angle 134(4)˚, in **SR-AI_S-Nap_A** and **RS-AI_S-Nap_A1** respectively).

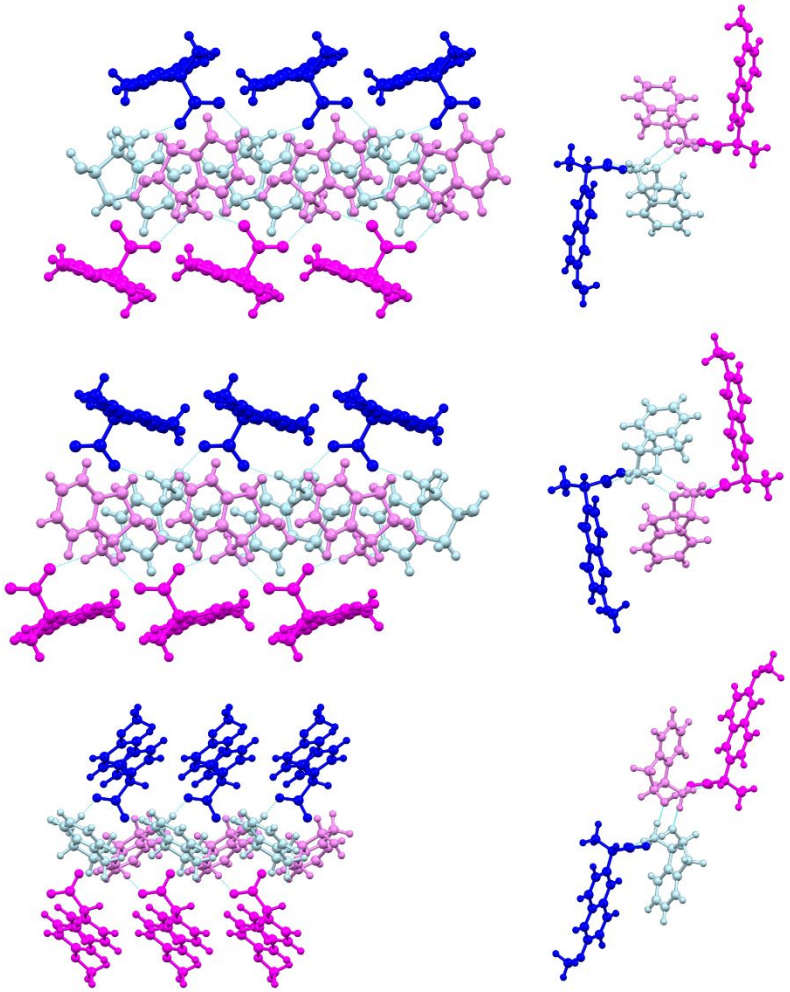

Figure 4. Intermolecular H-bonds within each column in **SR-AI_S-Nap_A** (top), **RS-AI_S-Nap_A1** (middle) and **RS-AI_S-Nap_A2** (bottom). Pink and blue colors are used to highlight ionic pairs related by the 2_1-screw axis. Left views along the *a*-axis direction, right views along the *b*-axis direction.

The same kind of interaction holds together different columns (Figure 5) through **AI**···**AI** and naproxen···naproxen interactions in **RS-AI_S-Nap_A1** (C7I-H7I···centroid distance 2.52(3)Å,

angle 156(4)°; C7-H7···centroid distance, 2.81(2)Å, angle 129(3)°, respectively); **AI**···naproxen and naproxen···naproxen in **RS-AI_S-Nap_A2** (C5-H5I···centroid distance 2.73(3)Å, angle 130(3)°, C14H14A···centroid distance 2.89(5) Å, angle 118(6)°); **AI**···**AI**, naproxen···naproxen and **AI**···naproxen ions in **SR-AI_S-Nap_A** (C7I-H7I···centroid distance 2.56(7)Å, angle 159(6)°; C7-H7···centroid distance 2.82(8)Å, angle 132(7)°; C9I-H9I···centroid distance 3.19(7)Å, angle 143(8)°, respectively).

As a result of these CH···π interactions, the stacked aryl groups of **AI** and naproxen ions describe herringbone motifs (face-to-edge).

Finally, in all the DSs a further inter-columns contact involves a methoxy hydrogen atom and a carboxylic oxygen atom in **SR-AI_S-Nap_A** and **RS-AI_S-Nap_A1** (C14-H14A···O1 2.45(8)Å, angle 136(7)° and C14-H14C···O1 2.78(5)Å, angle 140(6) °; respectively); while in **RS-AI_S-Nap_A2** the interaction involves the hydrogen atom provided by the methyl group bound to the asymmetric carbon atom (C9-H9B···O1 2.49(4)Å, angle 133(6) °).

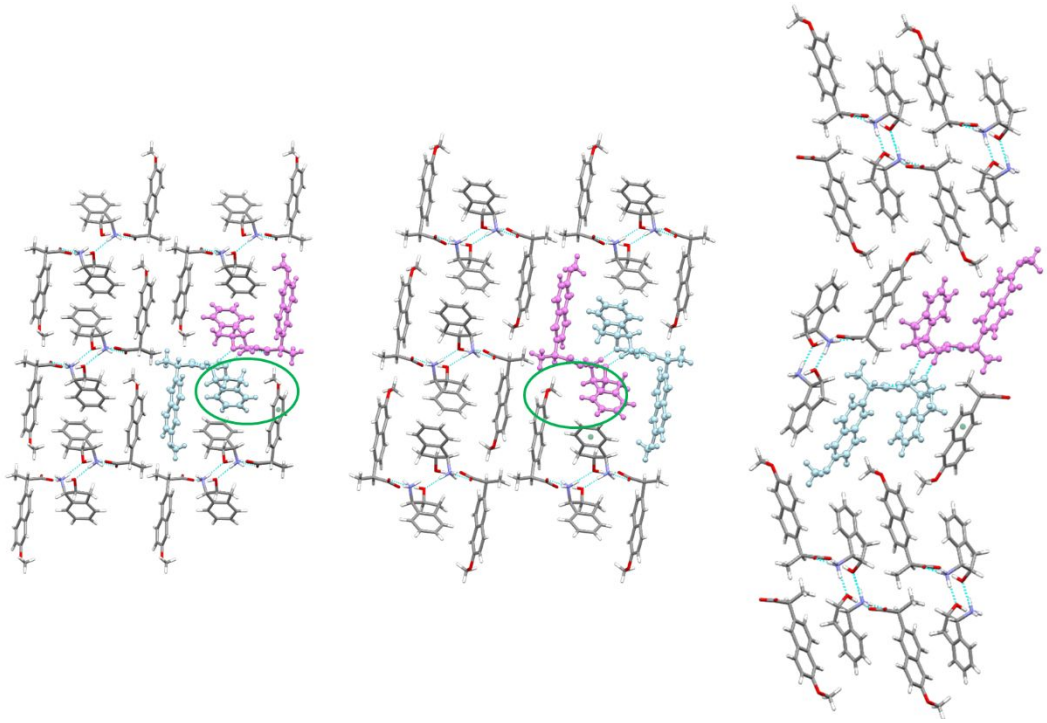

Figure 5. Crystal packing in **SR-AI_S-Nap_A** (left), **RS-AI_S-Nap_A1** (middle) and **RS-AI_S-Nap_A2** (right). The aromatic ring centroids help in evidencing the inter-column interactions; the green circle in **SR-AI_S-Nap_A** (left), **RS-AI_S-Nap_A1** (middle) evidence the relative position of aminoindanol and methoxy group of adjacent columns (see text).

As a final remark, at variance with **RS-AI_S-Nap_A2**, the **SR-AI_S-Nap_A** and **RS-AI_S-Nap_A1** crystal structures are characterized by layers of naproxen and aminoindanol which alternate parallel to the *ab* crystal face (Figure 6).

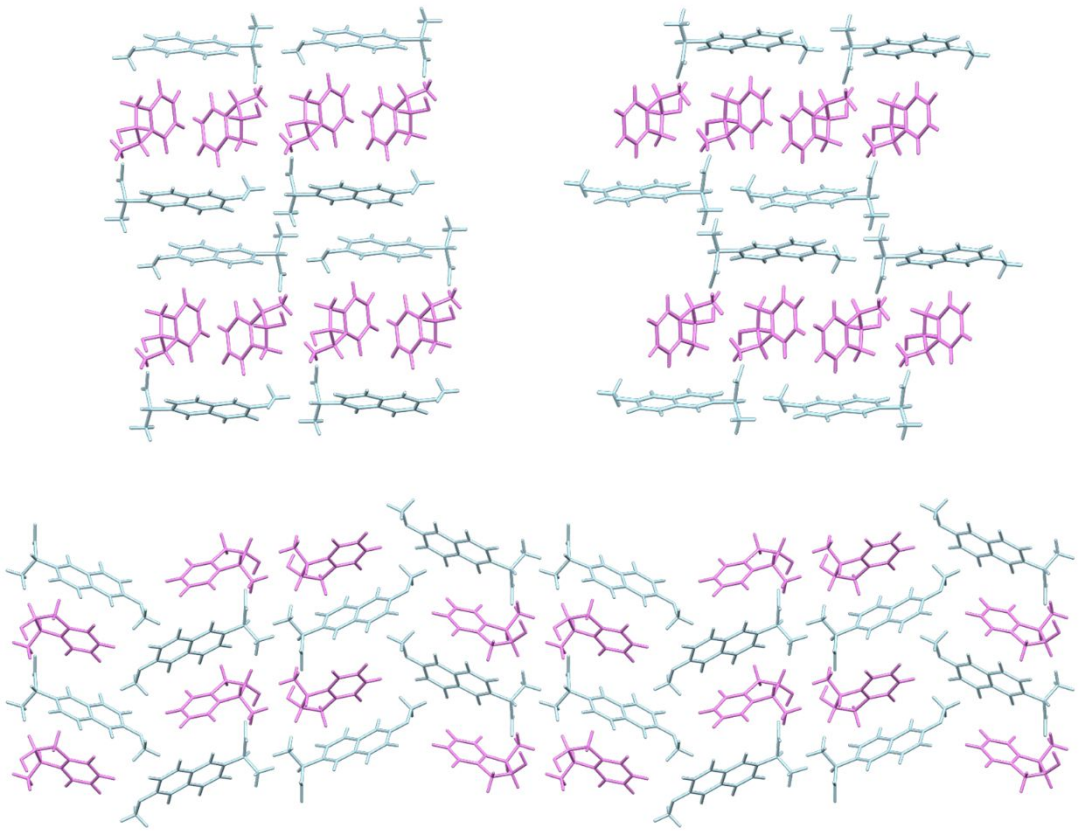

Figure 6. Layered structures of **SR-AI_S-Nap_A** (top left) and **RS-AI_S-Nap_A1** (top right) compared to the **RS-AI_S-Nap_A2** crystal packing (bottom). All structures are viewed along the *b*-axis direction.

In summary, the DSs crystal structures of **RS-AI_S-Nap_A1** and **SR-AI_S-Nap_A** mainly differ for the relative orientation of the aryl moieties of the ionic pair with respect to the $R_2^2(9)$ motif, i.e. *anti* (**RS-AI_S-Nap_A1**) and *syn* (**SR-AI_S-Nap_A**), being the overall crystal packing quite similar (layered structure). In addition, intra- and inter-column H-bonds and interactions are comparable in terms of type, number and geometry except for the lack of inter-

column CH···π contacts between the aminoindanol and naproxen ions in **RS-AI_S-Nap_A1**: the face-to-edge interaction fails because the candidate hydrogen atoms point toward the methoxy group (as evidenced by the green circle in Figure 5).

An identical H-bonds network ($R_2^2(9)$ and $R_4^3(11)$ motifs) hold together the two ionic partners in **RS-AI_S-Nap_A2**. However, the reduced D···A distances of the H-bond interactions (see Table 2) suggest a more robust columnar arrangement compared to both the **RS-AI_S-Nap_A1** solid form and the diastereomeric salt **SR-AI_S-Nap_A**. In addition, at variance with **RS-AI_S-Nap_A1**, in the ionic pair, the two H-bonded partners show a *syn* arrangement (as found in **SR-AI_S-Nap_A**). As for the CH···π interactions, they contribute to stabilize the crystal packing of **RS-AI_S-Nap_A2** *via* **AI**···naproxen and naproxen···naproxen intercolumns interactions.

The Hirshfeld Surface (HS) analysis was used to further study the crystal packing of the three DSs. As expected, the HSs of the naproxen anion mapped with $d_{norm,}$ show three large red spots related to the intermolecular H-bonds between the carboxylate oxygen atoms and the H-bond donors provided by the cation, a fourth definitely less pronounced spot reveals the CH···O interaction with an adjacent naproxen ion (Figure 7, top and Figure S11). As for the cations, in

all cases the HSs well evidence the involvement of all the potential H-bond donors and acceptors (3 large red spots for $-NH_3^+$ plus 2 for -OH) (Figure 7, bottom and Figure S11).

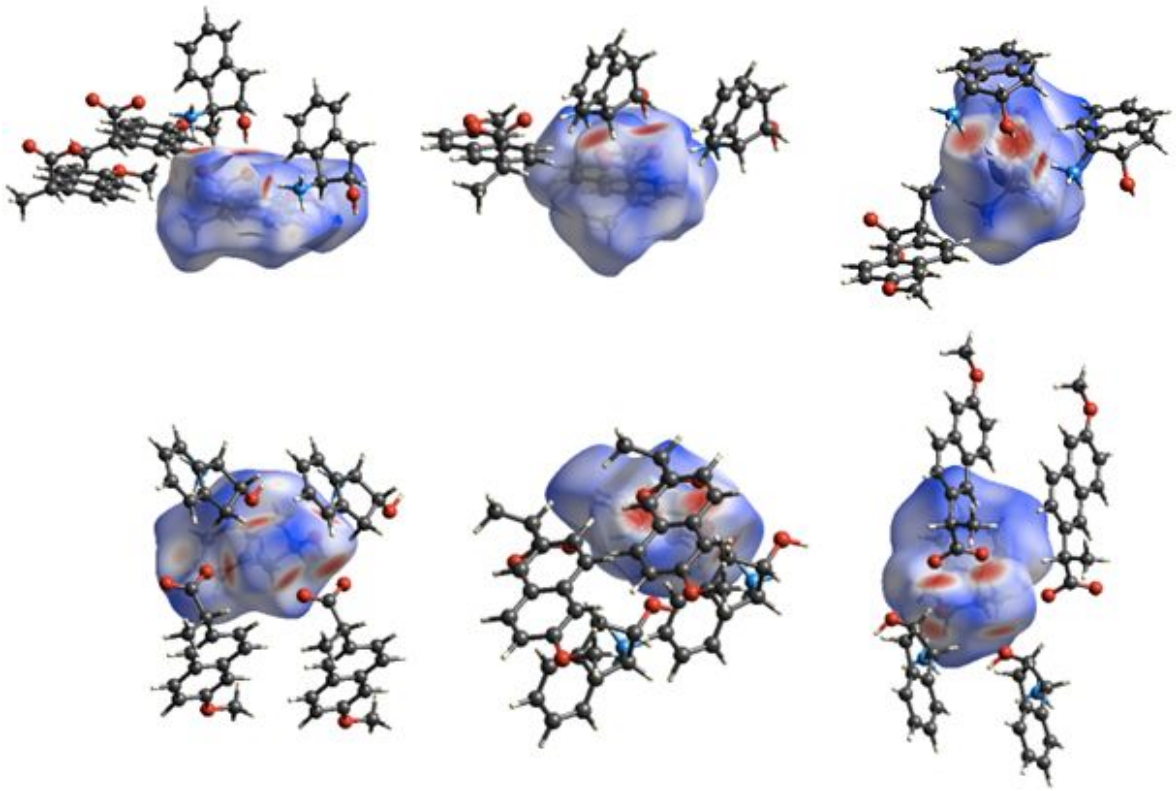

Figure 7. HSs of the naproxen anion (top) and aminoindanol cation (bottom) together with the closest interacting species in **SR-AI_S-Nap_A** (left), **RS-AI_S-Nap_A1** (middle) and **RS-AI_S-Nap_A2** (right).

The aminoindanol fingerprint plots are almost superimposable (see Figures S12-S14): the two sharp spikes highlight the O···H bonds involving the ammonium and hydroxyl moieties as H-bond donors (upper left, 18.9, 18.6 and 18.5% contribution to the **SR-AI_S-Nap_A, RS-AI_S-**

Nap_A1 and **RS-AI_S-Nap_A2** HSs, respectively) and the -OH group as acceptor (lower left, 4.7, 4.2 and 4.3% contribution to the **SR-AI_S-Nap_A, RS-AI_S-Nap_A1** and **RS-AI_S-Nap_A2** HSs, respectively). As for the naproxen fingerprint plots, those of **SR-AI_S-Nap_A** and **RS-AI_S-Nap_A1** are almost identical (see Figures S12 and S13), while that of **RS-AI_S-Nap_A2** (see Figure S14) shows some difference. O···H and C···H contributions to HSs are almost identical in **SR-AI_S-Nap_A** and **RS-AI_S-Nap_A1**, while in **RS-AI_S-Nap_A2** the contribution of these latter interactions is definitely greater, 27.4 vs 20.0%. In all cases the sharp and pronounced spike at the lower left (17.8 and 16.4% contribution to the HSs in **SR-AI_S-Nap_A** and **RS-AI_S-Nap_A1,** respectively) refers to the H-bonds involving the oxygen atoms provided by the carboxylate and methoxy groups; [62] the less evident spike at the upper left of the plots highlights the CH···O bonds (5.4, 4.9 and 3.6% contribution to the HSs in **SR-AI_S-Nap_A, RS-AI_S-Nap_A1** and **RS-AI_S-Nap_A2** respectively).

The asymmetric unit of the hydrated salt **RS-AI_S-Nap_W** contains two independent naproxen and 1-Amino-2-indanol ions and two water molecules. The overall shape of the naproxen, as well as that of the 1-Amino-2-indanol ions, is almost identical and definitely superimposable with that observed in the anhydrous **SR-AI_S-Nap_A** and **RS-AI_S-Nap_A1** (Figure S10). The independent naproxen anions are bridged through water molecules (see Table 3) which act as

H-bond donors towards one of the carboxylate oxygen atoms and -OCH_3. As a result, a ribbon of naproxen anions and water molecules propagates along the *b* axis direction (Figure 8, left).

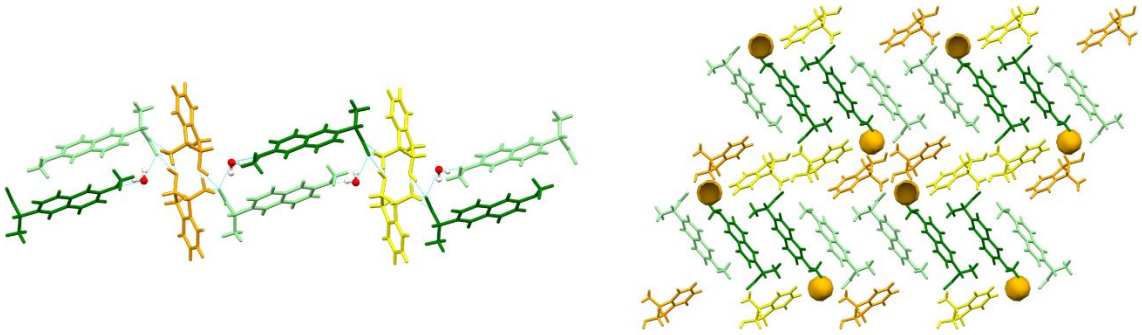

Figure 8. **RS-AI_S-Nap_W** crystal structure: ribbon motif (left) propagating along the *b* axis direction (dark and light green refer to the two independent naproxen anions, yellow and orange refer to the two independent indanol cations); isolated voids occupied by the water molecules (right).

Table 3. Selected interaction distances and angles in **RS-AI_S-Nap_W**

	H···Y distance (Å)	**X-H···Y angle (°)**
Interactions between naproxen anions and water molecules		
O1WA-H1W2···O2A	2.04(8)	150(6)°
O1WA-H1W1···O3B[1]	2.14(8)	153(7)
O1WB-H1W4···O2B	2.03(8)	150(7)

O1WB-H1W3···O3A	1.99(7)	166(7)
*Interactions between naproxen anions and **AI** cations*		
N1IA-H1NA···O1A[2]	1.82(5)	160(5)
N1IA-H1NB···O2A[3]	1.93(4)	175(3)
N1IB-H1NE···O1B	1.80(6)	164(5)
N1IB-H1NF···O2B[4]	1.89(4)	173(3)
O1IA-H1OA···O2A	1.76(1)	165(8)
O1IB-H1IB···O2B[5]	1.78(9)	161(8)°
Interactions between naproxen anions		
C6AH6A···O1A[1]	2.649(4)	169.1(4)
C6BH6B···O1B[1]	2.555(4)	171.4(4)

[1] = x,y-1,z; [2] = -x+2,y-1/2,-z+2; [3] = -x+2,y+1/2,-z+2; [4] = x,y+1,z; [5] = -x,y+1/2,-z+1

No additional H-bonds (as well evidenced by the corresponding HSs) involve the water molecules, which are lodged in isolated voids (Figure 8, right). Instead, **AI** cations bridge identical naproxen anions (related by translation along the *b*-axis direction) through NH···COO hydrogen bonds (see Table 3 and Figure 9 left), and 2_1 related anions via OH···COO hydrogen bonds (see Table 3). Due to such interactions, a layered crystal structure built by negatively charged ribbons (made of naproxen anions and water molecules) and aminoindanol cations resulted (Figure 9 right).

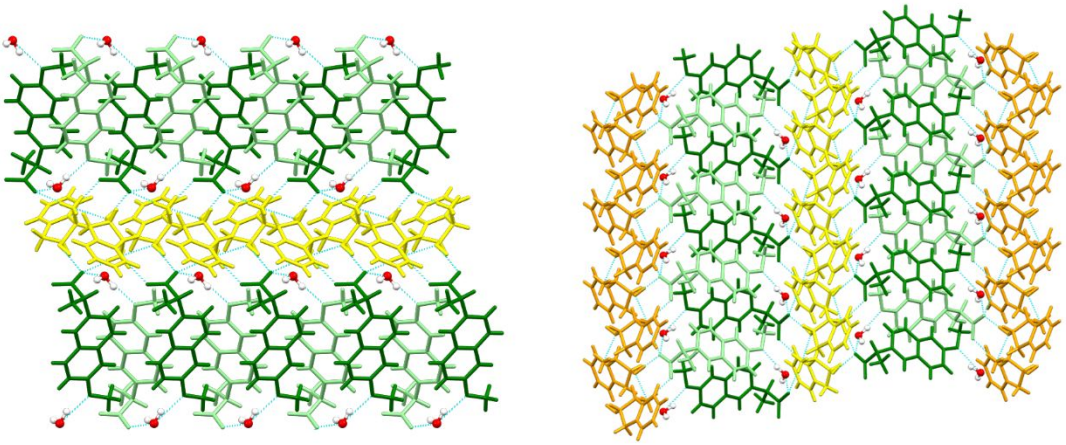

Figure 9. **RS-AI_S-Nap_W** crystal structure: aminoindanol cations bridging the naproxen anions (left) along the *b* axis direction (dark and light green refer to the two independent naproxen anions, yellow and orange refer to the two independent indanol cations); view along the c-axis direction of the alternating negative and positive layers (right).

In summary, each naproxen anion is strongly H-bound to three symmetry related **AI** cations and two independent water molecules (as also well evidenced by the deep red spots on the corresponding d_{norm} Hirshfeld surfaces); additional CH···OOC weak interactions bind identical naproxen anions along the *b*-axis direction (see Table 3). As for the **AI** cations, all the potential H-bond donors and acceptors contribute to build up the crystal packing as also consistently shown by the corresponding HSs. The contributions to the HSs, as provided by the corresponding fingerprint plots, do not significantly differ from those already reported for the anhydrous species **SR-AI_S-Nap_A** and **RS-AI_S-Nap_A1**.

Cambridge Structural Database (CSD) Survey

The search for crystal structures containing the cationic fragment depicted in Scheme 2 results in 22 hits; 14 of them were reported in Kinbara papers[45,46,63,64] as a part of his study of the chiral discrimination ability of 2-arylalkanoic acids by enantiopure 1-Amino-2-indanol and 1-Aminobenz[f]indan-2-ol resolving agents. 115 Hits were found from the search concerning the naproxen fragment, 2 of them involved an aminoindanol fragment (ELITIC[65], no 3D coordinates available, and YALWEO[64] refcodes).

The crystal structures of both the less- and more-soluble DSs made of SR-AI and 2-arylalkanoic acids (KAPVAY, KAPVEC; KAPWAZ, KAPYEF, KAPYIJ, KAPZOQ and KAQBAF refcodes) evidence the formation of a columnar hydrogen-bond network hold together by the ammonium and hydroxyl groups provided by **AI** and the acid carboxylate. Moreover, all the crystal packings are further reinforced by intra- and inter-column CH···π interactions which result in herringbone patterns. Kinbara reasoned that the differences in H-bonds and CH···π interactions strength could be responsible of the different stabilities which characterize the less- and more-soluble diastereomeric salt. For example, the crystal structures of the less soluble DS SR_AI-(R)-2-phenylbutyrate (KAPWAZ refcode) appear stabilized by hydrogen bonds

involving the hydroxyl group and herringbone packings much more than the corresponding more soluble SR_AI-(S)-2-phenylbutyrate (KAPYEF refcode). Furthermore, the crucial role of CH···π interactions, both intra- and inter-columnar, in chiral recognition was later examined by substituting the phenyl group in the indane skeleton of 1-Amino-2-indanol with a naphthyl group, yielding 1-Aminobenz[f]indan-2-ol. This substitution highlights the importance of a balanced control of these interactions to achieve enantioseparation.[63,64]

As for SR-AI, only two of the DSs studied by Kinbara,[45] *i.e.* KAPZOQ and KAQBAF, categorized as less-soluble and involving quite large α-alkyl groups on the 2-arylalkanoic acid, feature the $R_2^2(9)$motif as found in our DSs with naproxen. In particular the salt with (S)-2-methoxy-2-phenyl-2-(trifluoromethyl)acetate (KAQBAF) shows a 3D intra-column arrangement very similar to **SR-AI_S-Nap_A** and **RS-AI_S-Nap_A2**: "syn" arranged aromatic moieties and $R_4^3(11)$-H-bond motif (Figure 10). In his paper, Kinbara speculated that the steric repulsion between the α-substituents in the 2-arylalkanoic acids of KAPZOQ and KAQBAF and the aromatic moiety of AI, could be the reason of the slightly different H-bond pattern observed in these two cases with respect to the other acids of the series (α-alkyl group= -CH_3, -CH_2-CH_3), as well as of the absolute configuration of the carboxylate in the less-soluble

diastereomeric salts (the (S)-form of the 2-arylalkanoic acid was predominantly as the bulkiness of the alkyl group at the α-position increases).

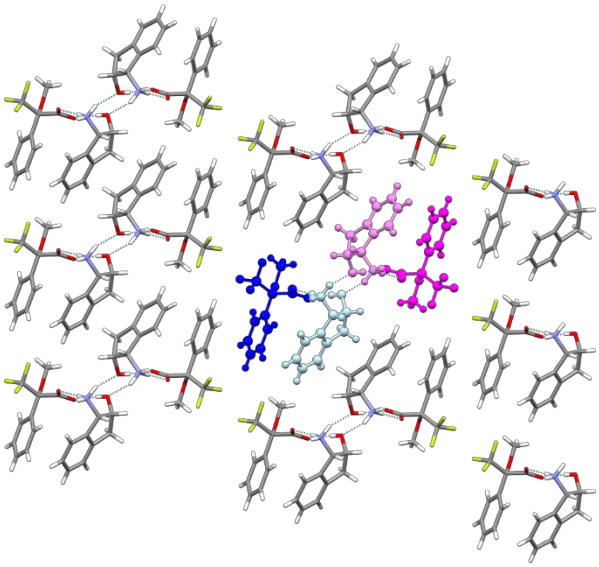

Figure 10. Crystal packing of (S)-2-methoxy-2-phenyl-2-(trifluoromethyl)acetate (KAQBAF) viewed along the *b*-axis direction.

A columnar hydrogen-bond network, extending along the 2_1 screw axis (Figure 11, top left), also characterizes the crystal structure of the already mentioned less-soluble salt of (S)-(+)-Naproxen with *trans*-1-Amino-2-indanol with (S)-(+)-Naproxen (OKIQAA refcode).[46] In this case, a H-bonded tetramer involving two **AI** (through the ammonium group) and two S-Nap ions can be recognized which can be categorized as $R_4^3(10)$, which is further reinforced by a hydrogen bond between the hydroxy group and a carboxylate oxygen atom originating an $R_2^1(7)$motif (Figure 11, top right). H-Bond distances and angles are comparable with those found

in **SR-AI_S-Nap_A** and **RS-AI_S-Nap_A2** (2.73-2.81 Å as for N···O and 149-165° as for NHO; 2.87 Å and 145° as for O···O and OHO). Moreover, intra- and inter-column CH···π interactions are present. Despite the different intra-column arrangement of the ionic partner, the resulting crystal packing closely resemble the layered structure which characterizes the **SR-AI_S-Nap_A** and **RS-AI_S-Nap_A1** species. (Figure 11, bottom).

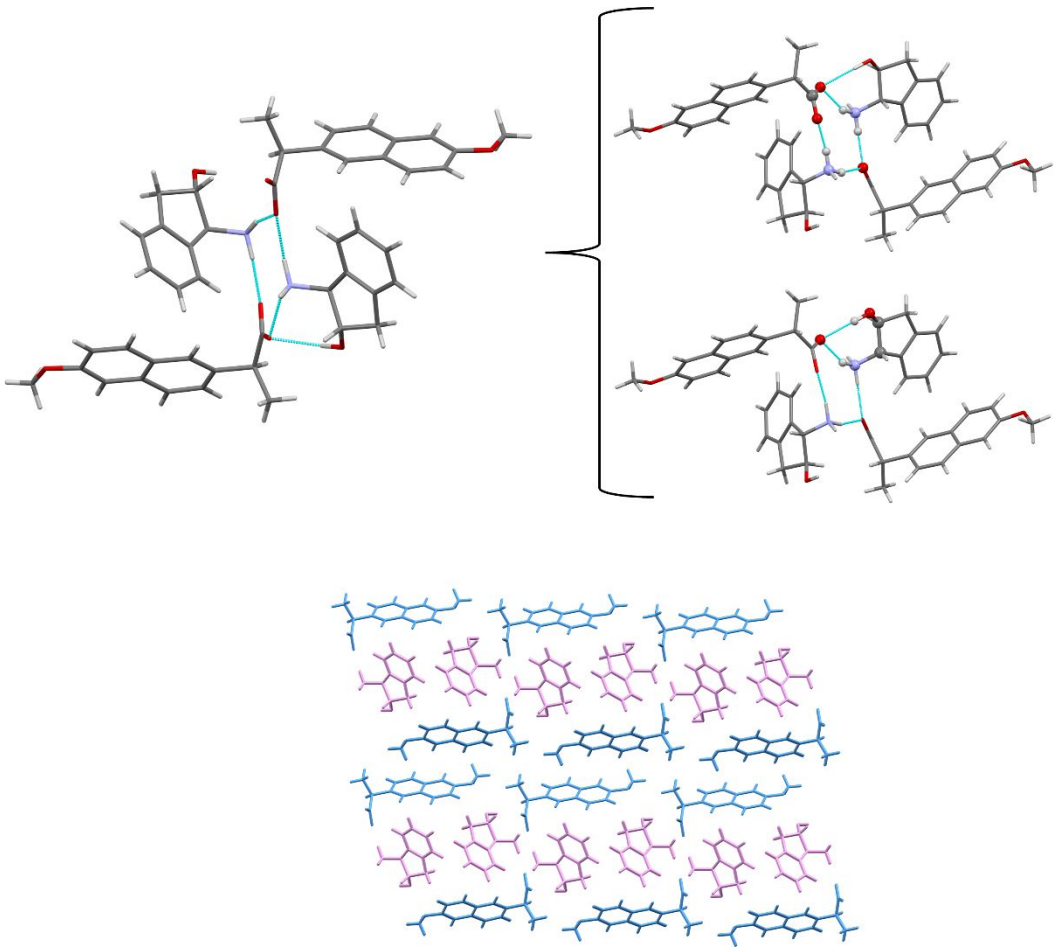

Figure 11. Crystal structure of (1S,2S)-trans-1-Aminoindan-2-ol (S)-2-(6-methoxy-2-naphthyl)propanoic acid (OKIQAA). Intermolecular H-bonds within each column viewed along the *b*-axis direction (top left); $R_4^3(10)$ and $R_2^1(7)$motifs in the reinforced H-bonded tetramer (top right); crystal packing viewed along the *b*-axis direction made of alternating layers of naproxen and aminoindanol ions parallel to the *ab* crystal face (bottom).

Selective crystallization experiments

In order to assess whether S-(+)-Naproxen was able to discriminate between the **AI** enantiomers, selectivity experiments were performed in solution. The experimental procedures adopted were similar to those used to obtain the pure DSs. Specifically, in all the three experiments performed (see Experimental section) the API was added to an equimolar solution of the two enantiomers while solvent composition (EtOH/H_2O: 4/1 or 2/1), temperature (r.t or reflux) and experiment time (few minutes or 1 h) were varied. In a short time (few minutes in the experiment performed at r.t., just after the cooling to r.t. in those performed at high

temperature) a precipitate formed which was immediately filtered out. In all cases the PXRD pattern identified the formation of the **SR-AI_S-Nap_A** salt (Figure S15).

DISCUSSION

As for the macroscopic solid forms behavior, results from the experiments reported in the previous chapters can be summarized as follows:

1) for the SR-AI/S-Nap salt, just one solid form (**SR-AI_S-Nap_A**) was observed notwithstanding the different synthetic procedures (*i.e.* solution, grinding, liquid-assisted grinding, solvent), and temperature/humidity conditions (*i.e.* changing the temperature no phase transformations were observed); 2) for the diastereomeric salt RS-AI/S-Nap two anhydrous phases (**RS-AI_S-Nap_A1** and **RS-AI_S-Nap_A2**) and one hydrated (**RS-AI_S-Nap_W**) were obtained depending on the synthetic procedures adopted and on the experimental conditions (*i.e.* a change in the temperature induced phase transformations); 3) the two anhydrous RS-AI/S-Nap solid forms are in monotropic relationship (the phase transition **RS-AI_S-Nap_A1→RS-AI_S-Nap_A2** is irreversible); 4) **RS-AI_S-Nap_W** dehydrates to **RS-AI_S-Nap_A2**; 5) all the anhydrous solid forms are stable (e.g. towards water uptake); 6)

preliminary selective crystallization experiments evidenced the preferential formation of the **SR-AI_S-Nap_A** salt.

From a crystal structure point of view, the three anhydrous DSs share as core characteristic a columnar arrangement of the ionic pairs held together by H-bonds ($R_2^2(9)$and $R_4^3(11)$motifs) which appears definitely more stable in **RS-AI_S-Nap_A2**. This observation is in keeping with the melting points of the two polymorphs (164 and 176° for **RS-AI_S-Nap_A1** and **RS-AI_S-Nap_A2**, respectively) and also with their Kitaigoroskii packing indices (K.P.I.) (67.7 vs 68.3 at 300K, respectively)[66]. On this basis, considering also the results from the solid-state investigation (points 2-5), we can speculate that **RS-AI_S-Nap_A1**, the less stable polymorphs, forms under kinetic control while **RS-AI_S-Nap_A2** is the thermodynamically stable solid form.

The **SR-AI_S-Nap_A** phase appears the preferred one, irrespective of the synthetic method and the environmental conditions applied (points 1 and 5), which suggests that SR-AI_S-Nap_A is the thermodynamically stable phase of the SR-AI/S-Nap salt. Selectivity tests (point 6) evidenced that, at least in our experimental conditions, the SR-AI/S-Nap salt was the first to form and to precipitate (**SR-AI_S-Nap_A** phase).This fact can be hardly rationalized on the basis of the different salts' (SR-AI/S-Nap and RS-AI/S-Nap) stabilities which result from

differences in H-bond and CH···π interaction strengths as suggested by Kinbara in a paper dealing with the discrimination of 2-arylalkanoic acids with (1*S*,2*R*)-cis-1-Amino-2-indanol.[45] In fact the in depth investigation of the crystal structures of **SR-AI_S-Nap_A** and **RS-AI_S-Nap_A1** (also complemented with data from CrystalExplorer analyses) suggests that both are sustained by intra-column and inter-columns interactions very similar in terms of nature and strength (except for the AI···nap interactions which in **RS-AI_S-Nap_A1** are missing). Moreover, almost identical packing arrangements (layers of alternating AI and naproxen ions) resulted as also reflected by the definitely equal values of the K.P.I. index (at 100K 69.4 and 69.2%, respectively). However, based on the melting temperature and enthalpy values, **SR-AI_S-Nap_A** appears by far the most stable anhydrous diastereomeric salt of the series (about 184˚C and ΔH = 85.7 kJ/mol *vs* 164˚C and ΔH = 37.9 kJ/mol for **RS-AI_S-Nap_A1**), with **RS-AI_S-Nap_A2** in the middle (melting temperature 176°C, melting enthalpy ΔH = 51.9 kJ/mol). **SR-AI_S-Nap_A** and **RS-AI_S-Nap_A2** have in common a *syn* arrangement of the charged partners with respect to the H-bonded $R_2^2(9)$ ring with respect to the *anti* one found in the **RS-AI_S-Nap_A1** solid form obtained under kinetic control. Could the *syn* arrangement and the additional CH···π inter-columns interactions involving the ionic partners found in **SR-AI_S-Nap_A** and **RS-AI_S-Nap_A2** be the decisive factors in determining the thermodynamic

stability of these two solid forms? Could they be crucial for the preferential formation of the **SR-AI_S-Nap_A** in the selective crystallization tests? On the other hand, it is well known that the stability of a given solid form depends on a subtle interplay of a lot of different attractive and repulsive interactions (as well shown by Kinbara's studies about CH···π interactions on very similar systems). Based on the collected data (for example the calculated cohesive energies of the three anhydrous DSs are within the expected errors), we are not able to conclusively answer the above question. Nonetheless this study adds a further piece to the very complicated puzzle of the relationships between structural characteristics and the chiral recognition mechanism.

CONCLUSION

In this paper we have presented the solid form landscape investigation of (S)-Naproxen / cis-1-Amino-2-indanol DSs by using a combination of experimental and *in-silico* methods. As for the RS-AI/S-Nap salt, two anhydrous phases (**RS-AI_S-Nap_A1**, **RS-AI_S-Nap_A2**) and one hydrated (**RS-AI_S-Nap_W**) were found, depending on the synthetic procedures adopted and on the experimental conditions. For example, on increasing the temperature, both the irreversible transformations **RS-AI_S-Nap_A1 -> RS-AI_S-Nap_A2** (the two polymorphs are

in a monotropic relationship) and the dehydration of **RS-AI_S-Nap_W** to **RS-AI_S-Nap_A2** occurred. By contrast, **SR-AI_S-Nap_A**, is the only solid form we were able to obtain for the SR-AI/S-Nap DS.

Preliminary chiral recognition ability tests of the enantiopure API for the racemic base evidenced the preferential formation of the **SR-AI_S-Nap_A** salt at least in our experimental conditions.

All the salts were structurally characterized by SCXRD (**SR-AI_S-Nap_A1**, **RS-AI_S-Nap_A1** and **RS-AI_S-Nap_W**) and PXRD (**RS-AI_S-Nap_A2**) The three anhydrous DSs shows a columnar arrangement of the ionic pairs held together by $R_2^2(9)$and $R_4^3(11)$H-bond motifs which seem more stable in **RS-AI_S-Nap_A2**, based on H-bond distances; in addition **SR-AI_S-Nap_A** and **RS-AI_S-Nap_A2** have in common a *syn* arrangement of the charged partners with respect to the $R_2^2(9)$ motif with respect to the *anti* one found in the **RS-AI_S-Nap_A1**. We speculated that **RS-AI_S-Nap_A1** is the less stable polymorphs, which forms under kinetic control while **RS-AI_S-Nap_A2** is the thermodynamically stable one (also in keeping with melting points trend and K.P.I. of the two polymorphs).

The in-depth study of the crystal structures of **SR-AI_S-Nap_A** and **RS-AI_S-Nap_A1** does not provide a convincing explanation of either the chiral discrimination ability of (S)-Naproxen

for SR-AI or the higher stability of the corresponding DS as suggested by the melting temperature and enthalpy. In fact, the DS crystal packings, which result in layers of alternating AI and naproxen ions, are very similar: both are held by intra-column and inter-columns interactions very similar in terms of nature and strength (almost identical K.P.I.) except for the AI···nap interactions which in **RS-AI_S-Nap_A1** are missing and the already cited *syn* vs *anti* arrangement within ionic pair. On the other hand, Kinbara's studies on very similar systems, highlighted that balancing intra- and inter-columnar CH···π interactions is crucial for a successful chiral discrimination.

To sum up the S-(+)-Naproxen / cis-1-Amino-2-indanol case further suggests that trying to rationalize on the basis of the crystal structure features the chiral discrimination process is a very complicated challenge, given that we are often dealing with structurally very similar DSs characterized by small differences, sometimes difficult to be spotted, which however could play a decisive role in determining stability differences in the DSs.

ASSOCIATED CONTENT

Supporting Information. The following files are available free of charge.

- CIF Files of **SR-AI_S-Nap_A, RS-AI_S-Nap_A1, RS-AI_S-Nap_A2, RS-AI_S-Nap_W**;

- DSC of **SR-AI_S-Nap_A, RS-AI_S-Nap_A1, RS-AI_S-Nap_W**;

-PXRD patterns;

- Superimposition of the naproxen anions as found in the crystal structures of the four crystalline phases (**SR-AI_S-Nap_A, RS-AI_S-Nap_A1, RS-AI_S-Nap_A2, RS-AI_S-Nap_W**);

- Fingerprint plots;

AUTHOR INFORMATION

Corresponding Author

Patrizia Rossi

Department of Industrial Engineering – University of Florence

Via Santa Marta 3, 50136 Florence (ITALY)

Email address = p.rossi@unifi.it

Author Contributions

The manuscript was written through contributions of all authors. All authors have given approval to the final version of the manuscript.

ACKNOWLEDGMENT

Authors thank CRIST (Centro di Servizi di Cristallografia Strutturale, University of Firenze-Italy) where the single-crystal X-ray analysis as well as all the rt PXRD experiments were carried out.

ABBREVIATIONS

cis-1-Amino-2-indanol = **AI**; (1R,2S)-cis-(+)-1-Amino-2-indanol = **RS-AI**; (1S,2R)-(-)-*cis*-1-Amino-2-indanol = **SR-AI**; (2*S*)-2-(6-methoxynaphthalen-2-yl)propanoic acid = **S-Nap**; (1S,2R)-(-)-cis-1-Ammonio-2-indanol (2S)-2-(6-methoxynaphtalen-2-yl)propionate, phase A = **SR-AI_S-Nap_A**; (1R,2S)-(+)-cis-1-Ammonio-2-indanol (2S)-2-(6-methoxynaphtalen-2-yl)propionate, phase A1 = **RS-AI_S-Nap_A1**; (1R,2S)-(+)-cis-1-Ammonio-2-indanol (2S)-2-(6-methoxynaphtalen-2-yl)propionate, phase A2 = **RS-AI_S-Nap_A2**; (1R,2S)-(+)cis-1-Ammonio-2-indanol (2S)-2-(6-methoxynaphtalen-2-yl)propionate hydrate = **RS-AI_S-**

Nap_W; Diastereomeric salt = DS; X-ray diffraction = XRD; Single Cystal X-ray diffraction = SCXRD; Powder X-ray diffraction = PXRD; Differential Scanning Calorimetry = DSC; Active Pharmaceutical Ingredient = API.

REFERENCES

(1) Nguyen, L. A.; He, H.; Pham-Huy, C. Chiral Drugs: An Overview. *International Journal of Biomedical Science* **2006**, 85–100.

(2) Lu, H. Stereoselectivity in Drug Metabolism. *Expert Opin Drug Metab Toxicol* **2007**, *3* (2), 149–158. https://doi.org/10.1517/17425255.3.2.149.

(3) Vargesson, N. Thalidomide-Induced Teratogenesis: History and Mechanisms. *Birth Defects Res C Embryo Today* **2015**, *105* (2), 140–156. https://doi.org/10.1002/bdrc.21096.

(4) Toda F. *Enantiomer Separation*; Toda, F., Ed.; Springer Netherlands: Dordrecht, 2004. https://doi.org/10.1007/978-1-4020-2337-8.

(5) Hadley, M. R. *Analysis of Drug Impurities*; Smith, R. J., Webb, M. L., Eds.; Blackwell: Tonbridge and Stevenage, UK, 2007.

(6) Jacques, J.; Collet, A.; Wilen, S. H. *Enantiomers, Racemates, and Resolutions*, John Wiley & Sons.; New York, 1981.

(7) Xiong, W. Q.; Lv, Y.; Peng, B.; Fu, S. G.; Duan, A. H.; Zhang, M.; Yuan, L. M. Enantioselective Resolutions by High-Performance Liquid Choromatography Using Chiral Inorganic Mesoporous Silica. *Sep Sci Plus* **2021**, *4* (2), 77–85. https://doi.org/10.1002/sscp.202000086.

(8) Mane, S. Racemic Drug Resolution: A Comprehensive Guide. *Analytical Methods* **2016**, *8* (42), 7567–7586. https://doi.org/10.1039/c6ay02015a.

(9) Hancu, G.; Orlandini, S.; Papp, L. A.; Modroiu, A.; Gotti, R.; Furlanetto, S. Application of Experimental Design Methodologies in the Enantioseparation of Pharmaceuticals by Capillary Electrophoresis: A Review. *Molecules* **2021**, *26* (15). https://doi.org/10.3390/molecules26154681.

(10) Tucker, G. T. Chiral Switches. *The Lancet* **2000**, *355*, 1085–1087.

(11) Agranat, I.; Caner, H.; Caldwell, J. Putting Chirality to Work: The Strategy of Chiral Switches. *Nat Rev Drug Discov* **2002**, *1* (10), 753–768. https://doi.org/10.1038/nrd915.

(12) Calcaterra, A.; D'Acquarica, I. The Market of Chiral Drugs: Chiral Switches versus de Novo Enantiomerically Pure Compounds. *J Pharm Biomed Anal* **2018**, *147*, 323–340. https://doi.org/10.1016/j.jpba.2017.07.008.

(13) Brooks, W. H.; Guida, W. C.; Daniel, K. G. The Significance of Chirality in Drug Design and Development. *Curr Top Med Chem* **2011**, *11*, 760–770.

(14) Teng, Y.; Gu, C.; Chen, Z.; Jiang, H.; Xiong, Y.; Liu, D.; Xiao, D. Advances and Applications of Chiral Resolution in Pharmaceutical Field. *Chirality* **2022**, *34* (8), 1094–1119. https://doi.org/10.1002/chir.23453.

(15) Sui, J.; Wang, N.; Wang, J.; Huang, X.; Wang, T.; Zhou, L.; Hao, H. Strategies for Chiral Separation: From Racemate to Enantiomer. *Chem Sci* **2023**. https://doi.org/10.1039/D3SC01630G.

(16) Ault, A. R(+)- and S(−)-α-Phenylehtylamine. *Org. Synt.* **1969**, *49*, 93–95.

(17) Van Eikeren, P.; McConville, F. X.; López, J. L. US19975677469. US19975677469, 1997.

(18) Sakurai, R.; Sakai, K. Resolution of Racemic Cis-1-Amino-2-Indanol by Diastereomeric Salt Formation with (S)-2-Phenylpropionic Acid. *Tetrahedron Asymmetry* **2003**, *14*, 411–413.

(19) Wu, H.; Jones, A. G. Crystallization, Dehydration, and Phase Transformations of Diastereomeric Salts: L-Ephedrine and D-Tartaric Acid. *Chem Eng Technol* **2012**, *35* (6), 1031–1038. https://doi.org/10.1002/ceat.201100683.

(20) Simon, M.; Donnellan, P.; Glennon, B.; Jones, R. C. Resolution via Diastereomeric Salt Crystallization of Ibuprofen Lysine: Ternary Phase Diagram Studies. *Chem Eng Technol* **2018**, *41* (5), 921–927. https://doi.org/10.1002/ceat.201700427.

(21) Pálovics, E.; Madarász, J.; Pokol, G.; Fogassy, E.; Bánhegyi, D. F. Economic Separations of Organic Acidic or Basic Enantiomeric Mixtures—A Protocol Suggestion. *Int J Mol Sci* **2023**, *24* (1). https://doi.org/10.3390/ijms24010846.

(22) Rossi, P.; Macedi, E.; Paoli, P.; Bernazzani, L.; Carignani, E.; Borsacchi, S.; Geppi, M. Solid-Solid Transition between Hydrated Racemic Compound and Anhydrous Conglomerate in Na-Ibuprofen: A Combined X-Ray Diffraction, Solid-State NMR, Calorimetric, and Computational Study. *Cryst Growth Des* **2014**, *14* (5), 2441–2452. https://doi.org/10.1021/cg500161e.

(23) Paoli, P.; Rossi, P.; Chelazzi, L.; Altamura, M.; Fedi, V.; Giannotti, D. Solid State Investigation and Characterization of a Nepadutant Precursor: Polymorphic and Pseudopolymorphic Forms of MEN11282. *Cryst Growth Des* **2016**, *16* (9), 5294–5304. https://doi.org/10.1021/acs.cgd.6b00826.

(24) Paoli, P.; Rossi, P.; Macedi, E.; Ienco, A.; Chelazzi, L.; Bartolucci, G. L.; Bruni, B. Similar but Different: The Case of Metoprolol Tartrate and Succinate Salts. *Cryst Growth Des* **2016**, *16* (2), 789–799. https://doi.org/10.1021/acs.cgd.5b01383.

(25) Rossi, P.; Paoli, P.; Chelazzi, L.; Conti, L.; Bencini, A. Metroprolol Fumarate: Crystal Structure from Powder X-Ray Diffraction Data and Comparison with the Tartrate and Succinate Salts. *Cryst Growth Des* **2018**, *18* (11), 7015–7026. https://doi.org/10.1021/acs.cgd.8b01182.

(26) Rossi, P.; Paoli, P.; Chelazzi, L.; Conti, L.; Bencini, A. The Solid-State Structure of the β-Blocker Metoprolol: A Combined Experimental and in Silico Investigation. *Acta Crystallogr C Struct Chem* **2019**, *75*, 87–96. https://doi.org/10.1107/S2053229618017084.

(27) Rossi, P.; Paoli, P.; Milazzo, S.; Chelazzi, L.; Ienco, A.; Conti, L. Investigating Differences and Similarities between Betaxolol Polymorphs. *Crystals (Basel)* **2019**, *9* (10), 509. https://doi.org/10.3390/cryst9100509.

(28) Paoli, P.; Milazzo, S.; Rossi, P.; Ienco, A. Rationalization of Lattice Thermal Expansion for Beta-Blocker Organic Crystals. *Crystals* **2020**, *10* (5), 350. https://doi.org/10.3390/cryst10050350.

(29) Paoli, P.; Lippi, M.; Milazzo, S.; Rossi, P.; Ceccarelli, J.; Chelazzi, L.; Ienco, A.; Conti, L. Molecular-Level Investigation of Hydrate-Anhydrous Phase Transformations of the Dapsone Structurally Related Compound 3,3′-Diaminophenyl Sulfone. *Cryst Growth Des* **2022**, *22* (12), 7176–7186. https://doi.org/10.1021/acs.cgd.2c00849.

(30) Araya-Sibaja, A. M.; Fandaruff, C.; Guevara-Camargo, A. M.; Vargas-Huertas, F.; Zamora, W. J.; Vega-Baudrit, J. R.; Guillén-Girón, T.; Navarro-Hoyos, M.; Paoli, P.; Rossi, P.; Jones, W. Crystal Forms of the Antihypertensive Drug Irbesartan: A Crystallographic, Spectroscopic, and Hirshfeld Surface Analysis Investigation. *ACS Omega* **2022**, *7* (17), 14897–14909. https://doi.org/10.1021/acsomega.2c00545.

(31) Córdova-Villanueva, E. N.; Rodríguez-Ruiz, C.; Sánchez-Guadarrama, O.; Rivera-Islas, J.; Herrera-Ruiz, D.; Morales-Rojas, H.; Höpfl, H. Diastereomeric Salt Formation by the γ-Amino Acid RS-Baclofen and L-Malic Acid: Stabilization by Strong Heterosynthons Based on Hydrogen Bonds between RNH3+ and COOH/COO- Groups. *Cryst Growth Des* **2018**, *18* (12), 7356–7367. https://doi.org/10.1021/acs.cgd.8b00990.

(32) Tumanova, N.; Seiler, V.; Tumanov, N.; Robeyns, K.; Filinchuk, Y.; Wouters, J.; Leyssens, T. Structural Analysis of D-Phenylglycinamide Salts Uncovers Potential Pitfalls in Chiral Resolution via Diastereomeric Salt Formation. *Cryst Growth Des* **2019**, *19* (7), 3652–3659. https://doi.org/10.1021/acs.cgd.8b01769.

(33) Sui, J.; Wang, N.; Wang, J.; Li, X.; Yang, J.; Liu, Y.; Zhao, Y.; Huang, X.; Wang, T.; Zhou, L.; Hao, H. Thermodynamic and Molecular Recognition Mechanism of Diastereomeric Salt/Cocrystal-Induced Chiral Separation. *Cryst Growth Des* **2022**, *22* (7), 4382–4395. https://doi.org/10.1021/acs.cgd.2c00355.

(34) Rossi, P.; Paoli, P.; Ienco, A.; Biagi, D.; Valleri, M.; Conti, L. A New Crystal Form of the NSAID Dexketoprofen. *Acta Crystallogr C Struct Chem* **2019**, *75*, 783–792. https://doi.org/10.1107/S2053229619006533.

(35) Rossi, P.; Paoli, P.; Chelazzi, L.; Milazzo, S.; Biagi, D.; Valleri, M.; Ienco, A.; Valtancoli, B.; Conti, L. Relationships between Anhydrous and Solvated Species of Dexketoprofen Trometamol: A Solid-State Point of View. *Cryst Growth Des* **2020**, *20* (1), 226–236. https://doi.org/10.1021/acs.cgd.9b01030.

(36) Rossi, P.; Paoli, P.; Milazzo, S.; Chelazzi, L.; Giovannoni, M. P.; Guerrini, G.; Ienco, A.; Valleri, M.; Conti, L. A Combined Crystallographic and Computational Study on Dexketoprofen Trometamol Dihydrate Salt. *Crystals* **2020**, *10* (8), 1–14. https://doi.org/10.3390/cryst10080659.

(37) Morais Missina, J.; Conti, L.; Rossi, P.; Ienco, A.; Gioppo Nunes, G.; Valtancoli, B.; Chelazzi, L.; Paoli, P. Ibuprofen as Linker for Calcium(II) in a 1D-Coordination Polymer: A Solid State Investigation Complemented with Solution Studies. *Inorganica Chim Acta* **2021**, *523*. https://doi.org/10.1016/j.ica.2021.120319.

(38) Rossi, P.; Ceccarelli, J.; Milazzo, S.; Paoli, P.; Morais Missina, J.; Ciattini, S.; Ienco, A.; Tuci, G.; Valleri, M.; Giovannoni, M. P.; Guerrini, G.; Conti, L. Nonsteroidal Anti-Inflammatory Drugs-1-Phenylethylamine Diastereomeric Salts: A Systematic Solid-State Investigation. *Cryst Growth Des* **2021**, *21* (12), 6947–6960. https://doi.org/10.1021/acs.cgd.1c00886.

(39) Gupta, A.; Bah, M. NSAIDs in the Treatment of Postoperative Pain. *Curr Pain Headache Rep* **2016**, *20* (11). https://doi.org/10.1007/s11916-016-0591-7.

(40) Budoff, P. W. Use of Mefenamic Acid in the Treatment of Primary Dysmenorrhea. *JAMA* **1979**, *241* (25), 2713–2716.

(41) Todd, P. A.; Clissold, S. P.; Wales, S.; Goldberg, M.; Sargent, J. Drug Evaluation Naproxen A Reappraisal of Its Pharmacology, and Therapeutic Use in Rheumatic Diseases and Pain States. *Drugs* **1990**, *40*, 91–137.

(42) Leung, G. J.; Rainsford, K. D.; Kean, W. F. Osteoarthritis of the Hand II: Chemistry, Pharmacokinetics and Pharmacodynamics of Naproxen, and Clinical Outcome Studies. *Journal of Pharmacy and Pharmacology* **2014**, *66* (3), 347–357. https://doi.org/10.1111/jphp.12165.

(43) Kinbara, K.; Sakai, K.; Hashimoto, Y.; Nohira ', H.; Saigo, K. Chiral Discrimination upon Crystallisation of the Diastereomeric Salts of 1-Arylethylamines with Mandelic Acid or p-Methoxymandelic Acid: Interpretation of the Resolution Efficiencies on the Basis of the Crystal Structures. *J. Chem. Soc., Perkin Trans. 2* **1996**, 2615-2622.

(44) Gallou, I.; Senanayake, C. H. Cis-1-Amino-2-Indanol in Drug Design and Applications to Asymmetric Processes. *Chem Rev* **2006**, *106* (7), 2843–2874. https://doi.org/10.1021/cr050970a.

(45) Kinbara, K.; Kobayashi, Y.; Saigo, K. Chiral Discrimination of 2-Arylalkanoic Acids by (1S,2R)-1-Aminoindan-2-Ol through the Formation of a Consistent Columnar Supramolecular Hydrogen-Bond Network †. *J. Chem. Soc* **2000**, 111–119.

(46) Kinbara, K.; Katsumata, Y.; Saigo, K. Chiral Discrimination of 2-Arylalkanoic Acids by (1S,2S)-1-Aminoindan-2-Ol and (1S,2S)-2-Aminoindan-1-Ol: Correlation of the Relative Configuration of the Amino and Hydroxy Groups with the Pattern of a Supramolecular Hydrogen-Bond Network in the Less-Soluble Diastereomeric Salt. *Chirality* **2003**, *15* (6), 564–570. https://doi.org/10.1002/chir.10202.

(47) Bruker (2012). Bruker APEX2. Bruker AXS Inc., Madison, Wisconsin, USA.

(48) Bruker (2012). Bruker SAINT; Bruker AXS Inc.: Madison, Wisconsin, USA.

(49) Burla, M. C.; Caliandro, R.; Camalli, M.; Carrozzini, B.; Cascarano, G. L.; De Caro, L.; Giacovazzo, C.; Polidori, G.; Spagna, R. SIR2004: An Improved Tool for Crystal Structure Determination and Refinement. *J Appl Crystallogr* **2005**, *38* (2), 381–388. https://doi.org/10.1107/S002188980403225X.

(50) Sheldrick, G. M. Crystal Structure Refinement with SHELXL. *Acta Crystallogr C Struct Chem* **2015**, *71*, 3–8. https://doi.org/10.1107/S2053229614024218.

(51) Nardelli, M. PARST95 - an Update to PARST: A System of Fortran Routines for Calculating Molecular Structure Parameters from the Results of Crystal Structure Analyses. *J. Appl. Crystallogr.* **1995**, *28*, 659. https://doi.org/https://doi.org/10.1107/S0021889895007138.

(52) Macrae, C. F.; Bruno, I. J.; Chisholm, J. A.; Edgington, P. R.; McCabe, P.; Pidcock, E.; Rodriguez-Monge, L.; Taylor, R.; Van De Streek, J.; Wood, P. A. Mercury CSD 2.0 - New Features for the Visualization and Investigation of Crystal Structures. *J Appl Crystallogr* **2008**, *41* (2), 466–470. https://doi.org/10.1107/S0021889807067908.

(53) Altomare, A.; Cuocci, C.; Giacovazzo, C.; Moliterni, A.; Rizzi, R.; Corriero, N.; Falcicchio, A. EXPO2013: A Kit of Tools for Phasing Crystal Structures from Powder Data. *J Appl Crystallogr* **2013**, *46* (4), 1231–1235. https://doi.org/10.1107/S0021889813013113.

(54) Brandenburg, J. G.; Caldeweyher, E.; Grimme, S. Screened Exchange Hybrid Density Functional for Accurate and Efficient Structures and Interaction Energies. *Physical Chemistry Chemical Physics* **2016**, *18* (23), 15519–15523. https://doi.org/10.1039/c6cp01697a.

(55) Dovesi, R.; Erba, A.; Orlando, R.; Zicovich-Wilson, C. M.; Civalleri, B.; Maschio, L.; Rérat, M.; Casassa, S.; Baima, J.; Salustro, S.; Kirtman, B. Quantum-Mechanical Condensed Matter Simulations with CRYSTAL. *Wiley Interdiscip Rev Comput Mol Sci* **2018**, *8* (4). https://doi.org/10.1002/wcms.1360.

(56) Coelho, A. A. TOPAS and TOPAS-Academic: An Optimization Program Integrating Computer Algebra and Crystallographic Objects Written in C++: An. *J Appl Crystallogr* **2018**, *51* (1), 210–218. https://doi.org/10.1107/S1600576718000183.

(57) Turner, M. J.; McKinnon, J. J.; Wolff, S. K.; Grimwood, D. J.; Spackman, P. R.; Jayatilaka, D.; Spackman, M. A. *CrystalExplorer17, Version 17*; University of Western Australia, Ed.; Crawley, Australia, 2017.

(58) Groom, C. R.; Bruno, I. J.; Lightfoot, M. P.; Ward, S. C. The Cambridge Structural Database. *Acta Crystallogr B Struct Sci Cryst Eng Mater* **2016**, *72* (2), 171–179. https://doi.org/10.1107/S2052520616003954.

(59) STARe, Thermal Analysis Software. Mettler - Toledo Int. Inc – Sonnenbergstrasse 74 – CH-8603 Schwerzenbahc, Switzerland.

(60) The sample used to obtain the pattern of the de-hydrated phase of **RS-AI_S-Nap_W** was obtained by putting a certain amount of **RS-AI_S-Nap_W** in an oven at 140°C for half an hour.

(61) Margaret Etter, B. C.; Macdonald, J. Graph-Set Analysis of Hydrogen-Bond Patterns in Organic Crystals. *Acta Crystallogr.* **1990**, *46*, 256–262. https://doi.org/https://doi.org/10.1107/S0108768189012929.

(62) **SR-AI_S-Nap_A**:C8H8···O3, 2.75(6)A, 139(5)° **RS-AI_S-Nap_A1**:C8H8···O3, 2.77(4)A, 146(3).

(63) Kobayashi, Y.; Kurasawa, T.; Kinbara, K.; Saigo, K. Rational Design of CH/π Interaction Sites in a Basic Resolving Agent. *Journal of Organic Chemistry* **2004**, *69* (22), 7436–7441. https://doi.org/10.1021/jo049154d.

(64) Kobayashi, Y.; Kinbara, K.; Sato, M.; Saigo, K. Synthesis, Absolute Configuration, and Application of Enantiopure Trans-1-Aminobenz[f]Indan-2-Ol. *Chirality* **2005**, *17* (2), 108–112. https://doi.org/10.1002/chir.20101.

(65) Kinbara, K.; Katsumata, Y.; Saigo, K. Enantiopure Trans-and Cis-3-Aminoindan-1-Ols: Preparation and Application as Novel Basic Resolving Agents. *Chem Lett* **2002**, *31* (3), 266–267.

(66) Kitaigorodskii, A. I. *Organic Chemical Crystallography*; Consultants Bureau, Ed.; New York, 1961.

"For Table of Contents Only"

The same but not the same: the case of (S)-Naproxen / cis-1-Amino-2-indanol chiral resolution via diastereomeric salt formation

Martina Lippi, Patrizia Rossi, Jacopo Ceccarelli, Stella Milazzo, Juliana Morais Missina, Andrea Ienco, Luca Conti, Laura Chelazzi, Paola Paoli*

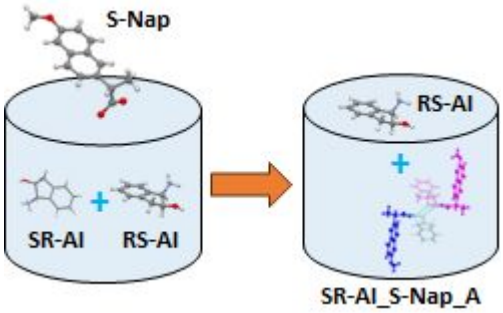

Synopsis:

To explore the preference of S-(+)-Naproxen for one of the cis-1-Amino-2-indanol enantiomers and gain insights into the forces driving the chiral discrimination process, the solid-state structures of four diastereomeric salts was investigated and comprehensive experimental and in-silico analyses were carried out.

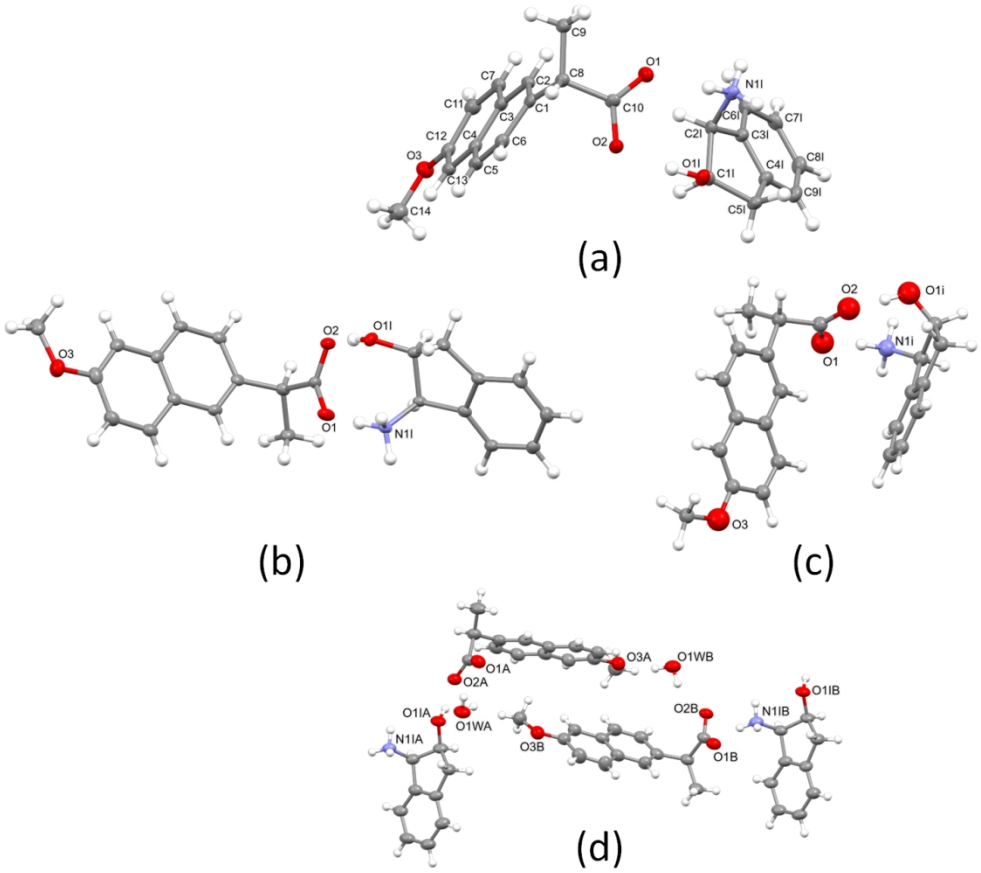

Figure 1. Views of the asymmetric unit of **SR-AI_S-Nap_A** (top), **RS-AI_S-Nap_A1** (middle, left), **RS-AI_S-Nap_A2** (middle, right) and **RS-AI_S-Nap_W** (bottom). For **SR-AI_S-Nap_A**, **RS-AI_S-Nap_A1** and **RS-AI_S-Nap_W** ORTEP views with 50% ellipsoid probability are shown, while for **RS-AI_S-Nap_A2** a ball and stick model is used. The atoms labelling scheme adopted is the same for all the structures and, for the sake of clarity, reported (except for the hydrogen atoms) for **SR-AI_S-Nap_A**, while in the other three structures only the nitrogen and oxygen labels are shown.

123x110mm (300 x 300 DPI)

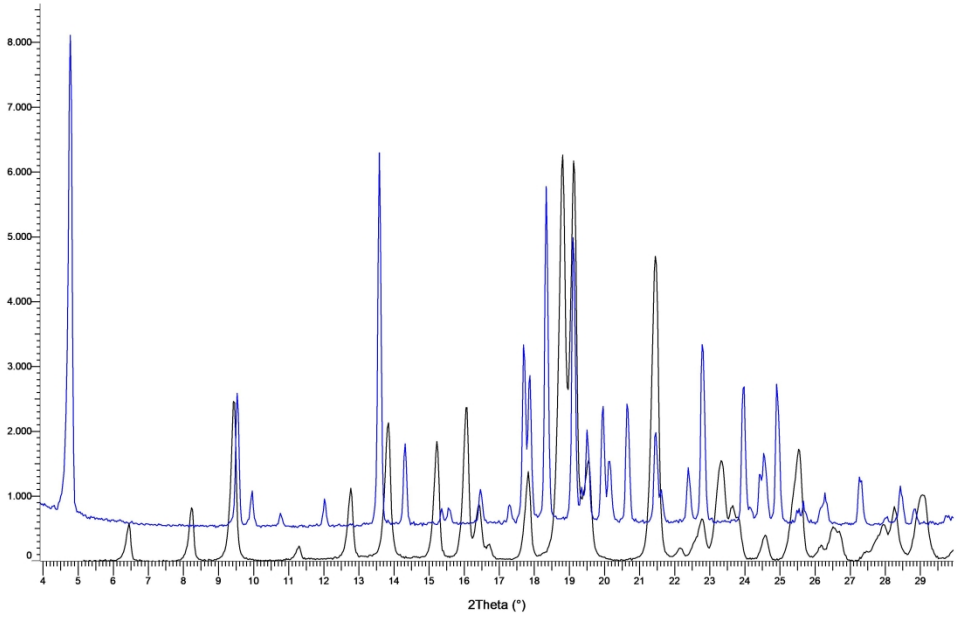

Figure 2. Superimposition of the PXRD pattern of RS-AI_S-Nap at the beginning (black) and at the end (blue) of the oven experiment.

341x218mm (300 x 300 DPI)

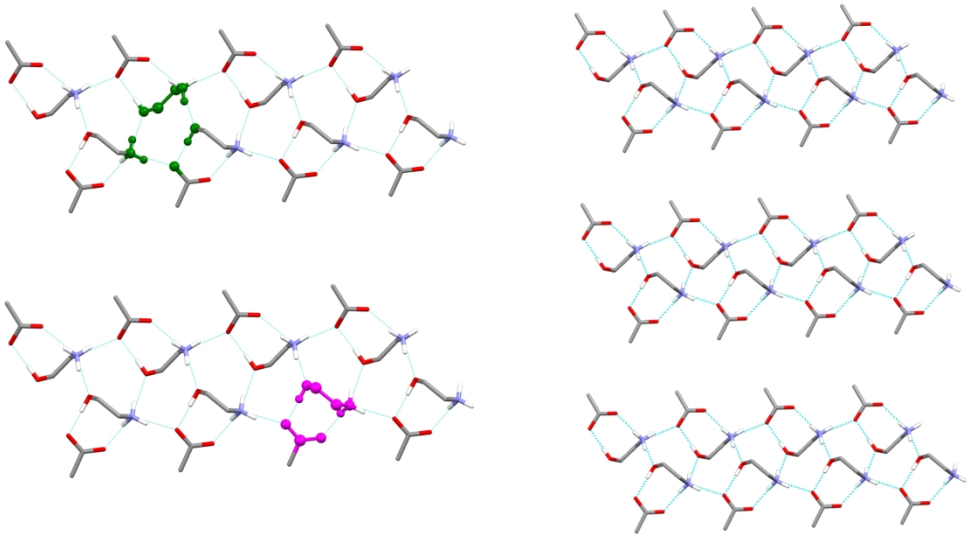

Figure 3. Schematic drawing of the H-bond network in the naproxen diastereomeric salts evidencing the R2,2(9) (ball and stick, pink) and R3,4(11) (ball and stick, green) H-bond motifs view along the a-axis direction. Left: columnar H-bond network; right: columns packing. Figure refers to **SR-AI_S-Nap_A**.

222x121mm (300 x 300 DPI)

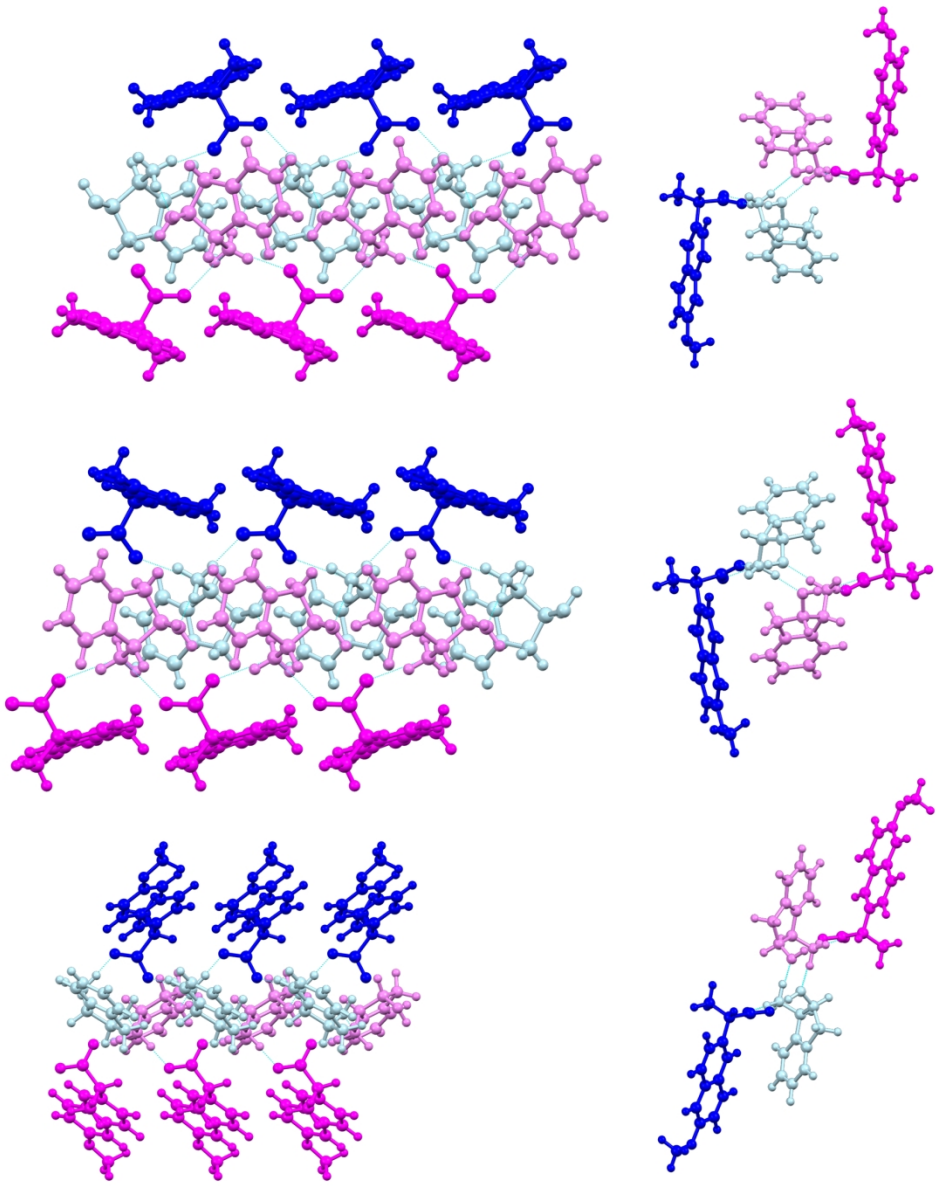

Figure 4. Intermolecular H-bonds within each column in **SR-AI_S-Nap_A** (top), **RS-AI_S-Nap_A1** (middle) and **RS-AI_S-Nap_A2** (bottom). Pink and blue colors are used to highlight ionic pairs related by the 21-screw axis. Left views along the a-axis direction, right views along the b-axis direction.

160x198mm (300 x 300 DPI)

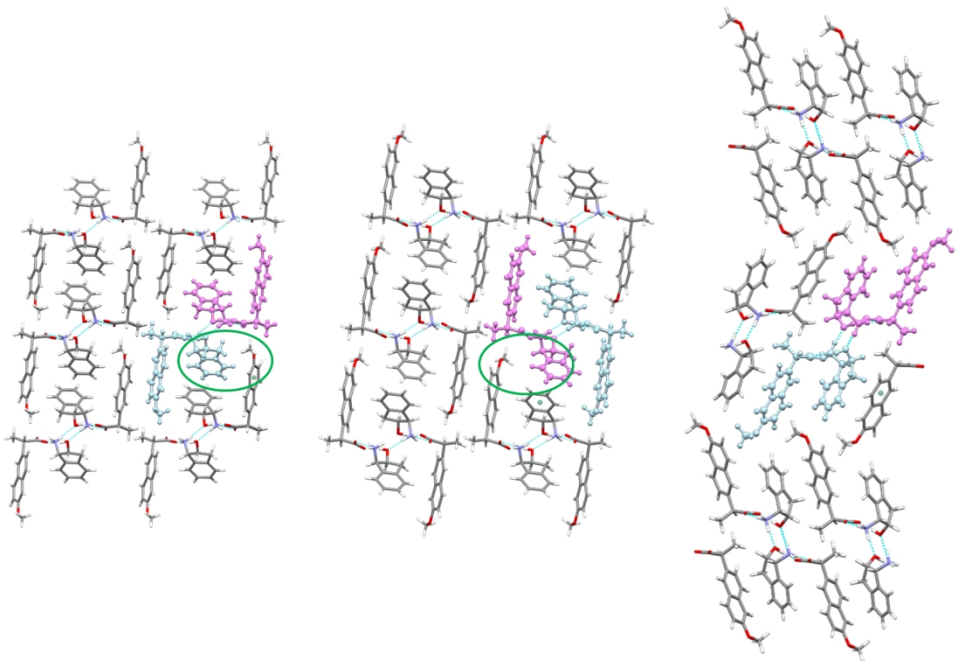

Figure 5. Crystal packing in **SR-AI_S-Nap_A** (left), **RS-AI_S-Nap_A1** (middle) and **RS-AI_S-Nap_A2** (right). The aromatic ring centroids help in evidencing the inter-column interactions; the green circle in **SR-AI_S-Nap_A** (left), **RS-AI_S-Nap_A1** (middle) evidence the relative position of aminoindanol and methoxy group of adjacent columns (see text).

144x94mm (300 x 300 DPI)

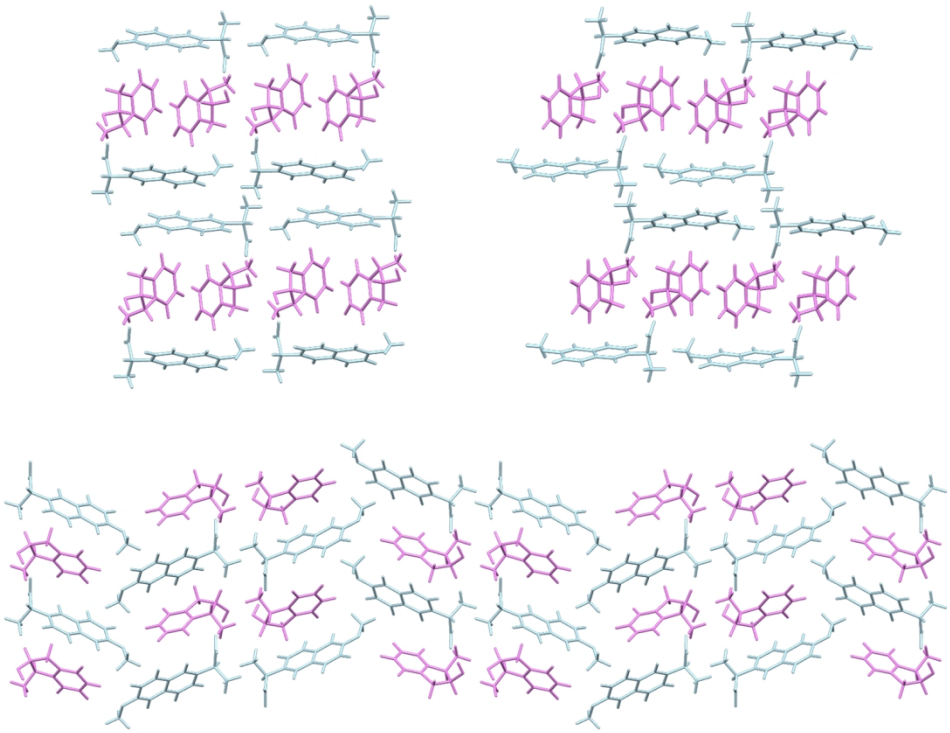

Figure 6. Layered structures of **SR-AI_S-Nap_A** (top left) and **RS-AI_S-Nap_A1** (top right) compared to the **RS-AI_S-Nap_A2** crystal packing (bottom). All structures are viewed along the b-axis direction.

143x113mm (300 x 300 DPI)

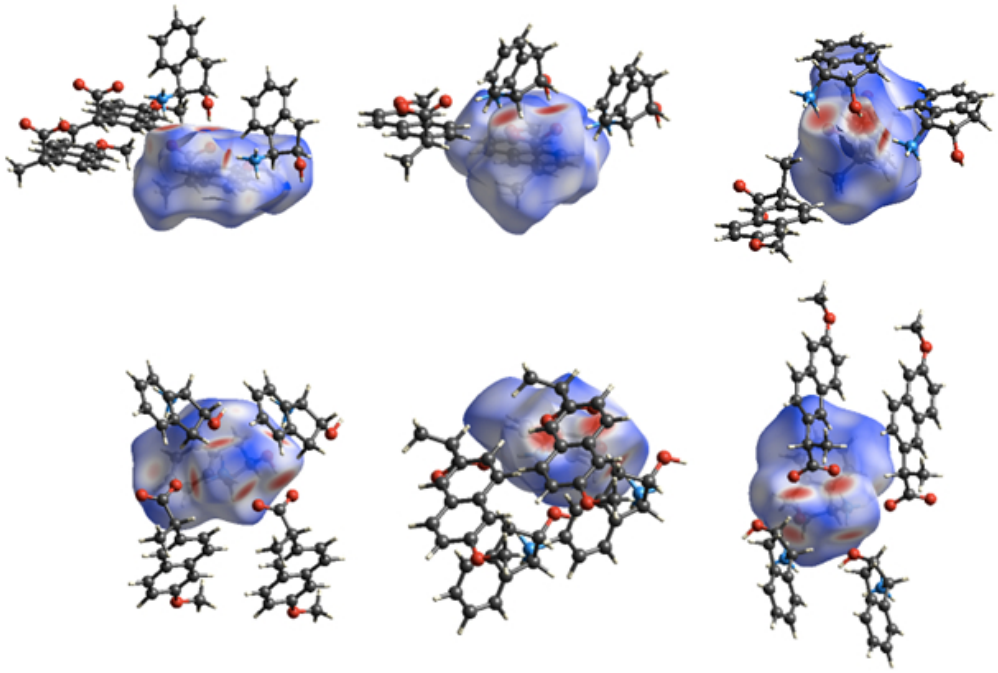

Figure 7. HSs of the naproxen anion (top) and aminoindanol cation (bottom) together with the closest interacting species in **SR-AI_S-Nap_A** (left), **RS-AI_S-Nap_A1** (middle) and **RS-AI_S-Nap_A2** (right).

51x34mm (300 x 300 DPI)

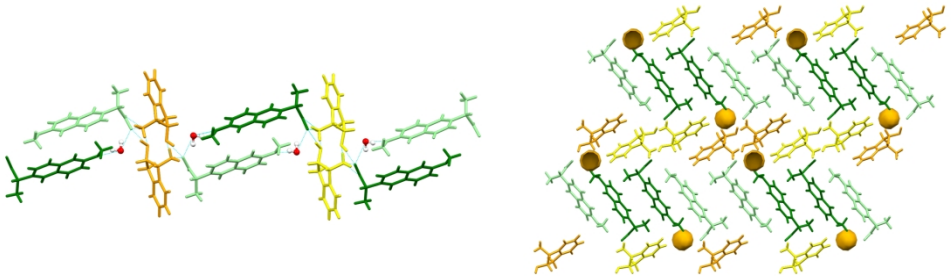

Figure 8. **RS-AI_S-Nap_W** crystal structure: ribbon motif (left) propagating along the b axis direction (dark and light green refer to the two independent naproxen anions, yellow and orange refer to the two independent indanol cations); isolated voids occupied by the water molecules (right).

212x60mm (300 x 300 DPI)

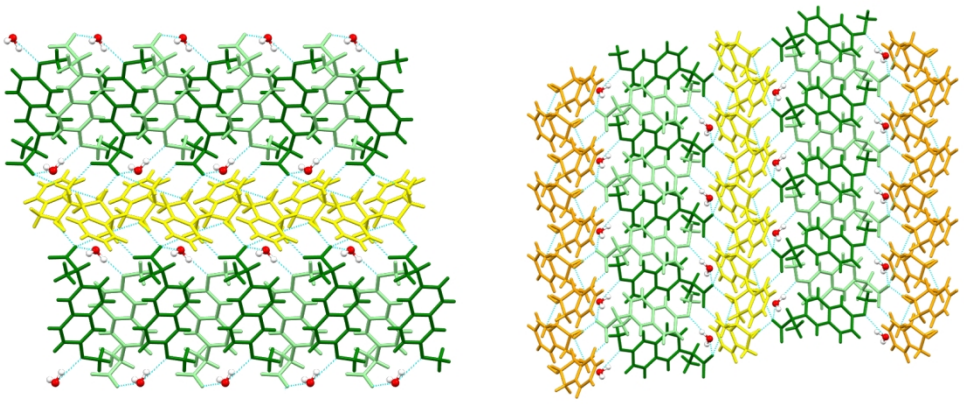

Figure 9. **RS-AI_S-Nap_W** crystal structure: aminoindanol cations bridging the naproxen anions (left) along the b axis direction (dark and light green refer to the two independent naproxen anions, yellow and orange refer to the two independent indanol cations); view along the c-axis direction of the alternating negative and positive layers (right).

146x60mm (300 x 300 DPI)

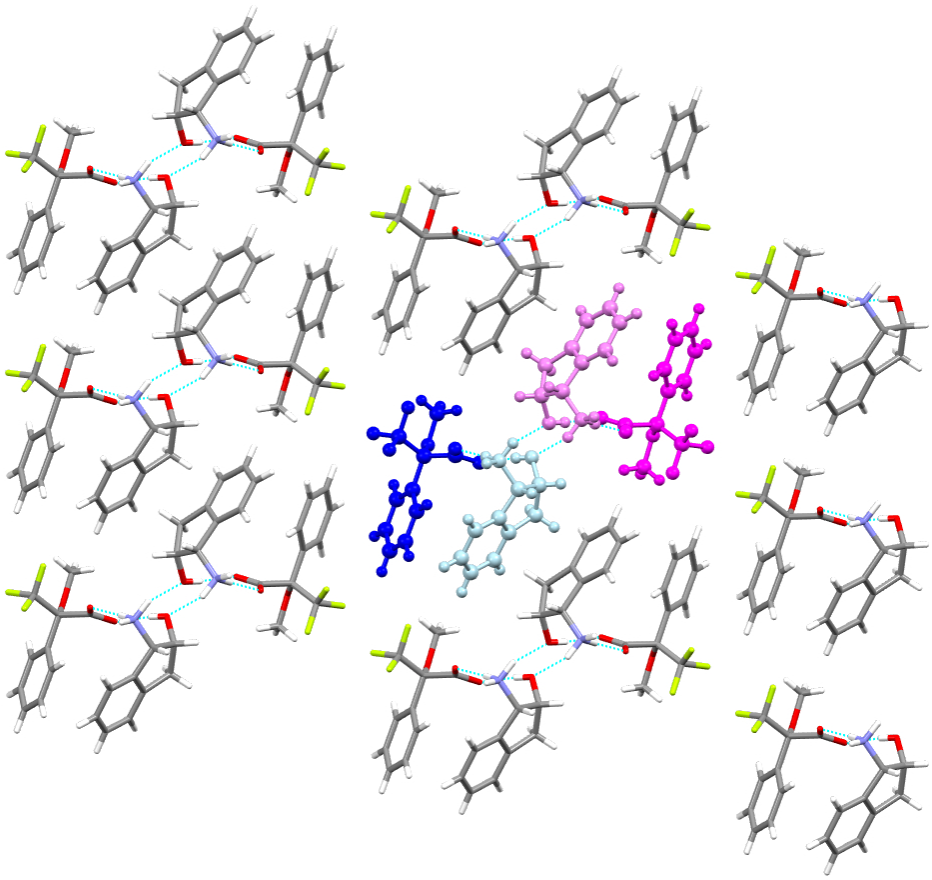

Figure 10. Crystal packing of (S)-2-methoxy-2-phenyl-2-(trifluoromethyl)acetate (KAQBAF) viewed along the b-axis direction.

84x74mm (300 x 300 DPI)

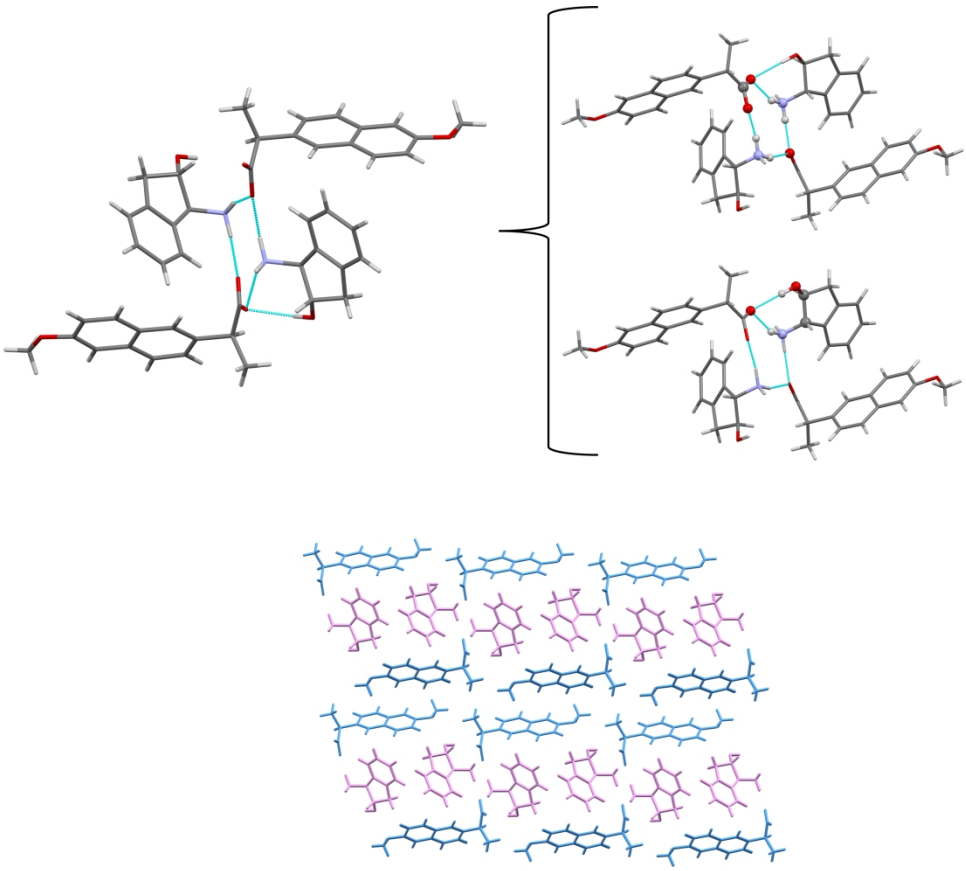

Figure 11. Crystal structure of (1S,2S)-trans-1-Aminoindan-2-ol (S)-2-(6-methoxy-2-naphthyl)propanoic acid (OKIQAA). Intermolecular H-bonds within each column viewed along the b-axis direction (top left); R3,4(10) and R1,2(7) motifs in the reinforced H-bonded tetramer (top right); crystal packing viewed along the b-axis direction made of alternating layers of naproxen and aminoindanol ions parallel to the ab crystal face (bottom).

255x220mm (300 x 300 DPI)

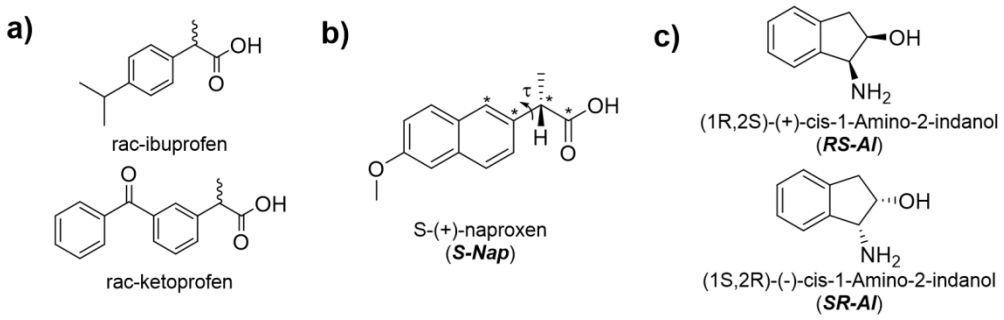

Scheme 1. a) Schematical drawing of Ibuprofen and Ketoprofen; b) Schematical drawing of (S)-(+)-Naproxen (**S-Nap**) with evidenced the atoms defining the torsion angle □; c) Schematical drawing of (1R,2S)-(+)-cis-1-Amino-2-indanol (**RS-AI**) and (1S,2R)-(-)-cis-1-Amino-2-indanol (**SR-AI**).

140x44mm (300 x 300 DPI)

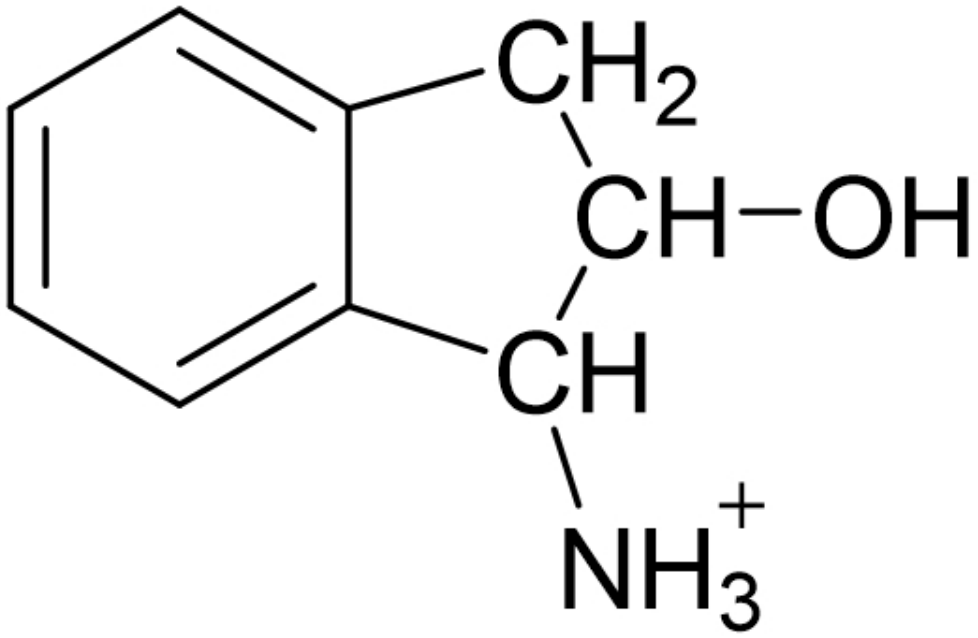

Scheme 2. 1-Amino-2-indanol fragment searched in the Cambridge Structural Database.

45x29mm (300 x 300 DPI)

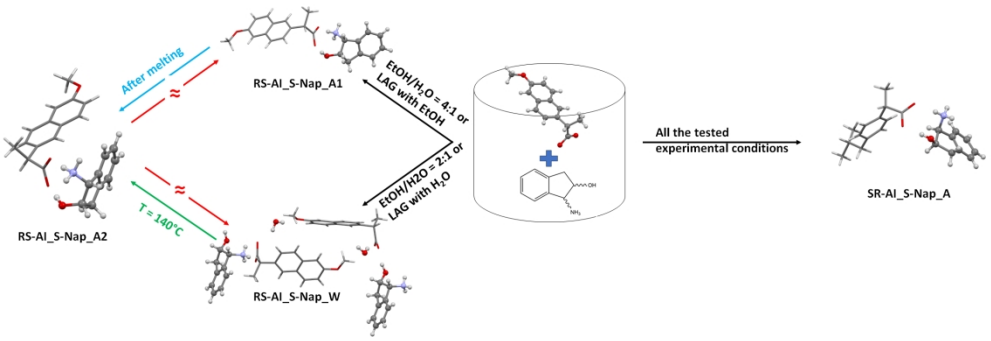

Scheme 3. Solid forms formation conditions and relationships.

204x69mm (300 x 300 DPI)